Metabolic reconstitution by a gnotobiotic microbiota varies over the circadian cycle

Authors:

- Hoces, Daniel[1]
- Lan, Jiayi[2]
- Wenfei, Sun[3]
- Geiser, Tobias[1]
- Cappio, Elisa[1]
- Arnoldini, Markus[1]
- Nowok, Sven[4]
- Macpherson, Andrew J[5]
- Stecher, Bärbel[6,7]
- Zenobi, Renato[2]
- Hardt, Wolf-Dietrich[8]
- Wolfrum, Christian[3]
- Slack, Emma[1,9]

1. Laboratory for Food Immunology, Institute of Food, Nutrition and Health, Department of Health Sciences and Technology, ETH Zürich, 8093 Zürich, Switzerland
2. Laboratory of Organic Chemistry, Department of Chemistry and Applied Biosciences, ETH Zürich, 8093 Zürich, Switzerland
3. Laboratory of Translational Nutrition Biology, Institute of Food, Nutrition and Health, Department of Health Sciences and Technology, ETH Zürich, 8603 Schwerzenbach, Switzerland
4. ETH Phenomics Center, Department of Biology, ETH Zürich, 8093 Zürich, Switzerland

5. Department of Biomedical Research, Gastroenterology & Mucosal Immunology, University of Bern, 3010 Bern, Switzerland
6. Max-von-Pettenkofer Institute, LMU Munich, Munich, Germany
7. German Center for Infection Research (DZIF), partner site LMU Munich, 80539 Munich, Germany
8. Institute of Microbiology, Department of Biology, ETH Zürich, 8093 Zürich, Switzerland
9. Corresponding author. Email: emma.slack@hest.ethz.ch

SUMMARY

The capacity of the intestinal microbiota to degrade otherwise indigestible diet components is known to greatly improve the recovery of energy from food. This has led to the hypothesis that increased digestive efficiency may underlie the contribution of the microbiome to obesity. OligoMM12-colonized gnotobiotic mice have a consistently higher fat-mass than germ-free or fully colonized counterparts. We therefore investigated their food intake, digestion efficiency, energy expenditure and respiratory quotient using a novel isolator-housed metabolic cage system which allows long-term measurements without contamination risk. This demonstrated that microbiota-released calories are perfectly balanced by decreased food intake in fully colonized versus gnotobiotic OligoMM12 and germ-free mice fed a standard chow diet, i.e., microbiota-released calories can in fact be well-integrated into appetite control. We also observed no significant difference in energy expenditure per gram lean mass between the different microbiota groups, suggesting that cumulative very small differences in energy balance, or altered energy storage must underlie fat accumulation in OligoMM12 mice. Consistent with altered energy storage, major differences were observed in the type of respiratory substrates used in metabolism over the circadian cycle: in germ-free mice the respiratory exchange ratio was consistently lower than that of fully colonized mice at all times of day, indicative of more reliance on fat and less on glucose metabolism. Intriguingly OligoMM12-colonized gnotobiotic mice phenocopied fully colonized mice during the dark (active/eating) phase but phenocopied germ-free mice during the light (fasting/resting) phase. The liver metabolome of OligoMM12 mice also clusters very tightly with germ-free mice during the light-phase and shifts to be closer to colonized animals during the dark-phase. This indicates the existence of microbiota functions that are specifically required to maintain normal host metabolism during the resting/fasting phase of circadian cycle, and which are selectively absent in the OligoMM12 consortium.

KEYWORDS

Microbiota, Host Metabolism, Gnotobiotic, Circadian rhythm.

INTRODUCTION

The gut microbiota is currently considered a key regulator of host energy metabolism (Sonnenburg and Bäckhed, 2016). In the absence of a microbiota, mice accumulated less fat (Bäckhed et al., 2004) and were protected from obesity induced by certain types of high-fat diets (Bäckhed et al., 2007; Fleissner et al., 2010; Kübeck et al., 2016). Several mechanisms have been proposed to explain this phenomenon and its relationship to metabolic imbalances (Cani et al., 2019). These include endocrine regulation of food intake (Goswami et al., 2018; Lin et al., 2012), additional energy liberated by the microbiota from dietary fibers (Turnbaugh et al., 2006), alterations in bile acid profiles (Sayin et al., 2013; Yao et al., 2018), inflammatory responses induced by some members of the microbiota (Caesar et al., 2015) and induction of thermogenesis in adipose tissue (Krisko et al., 2020; Li et al., 2019, 2021). However, given the complexity of a complete microbiota and its interactions with the host, validating any of these theories and identifying causal relationships remains a major experimental challenge (Harley and Karp, 2012; Walter et al., 2020).

Gnotobiotic mice, colonized with a simplified microbiota made up of defined species, have become a major tool to identify potential mechanisms of interaction between the microbiota and host (Koh and Bäckhed, 2020; Mallapaty, 2017; Steimle et al., 2021). Such approaches can generate a mechanistic understanding of how external factors (i.e. diet, infection) act on the different microbiota members individually and at a community level (Faith et al., 2014; Kovatcheva-Datchary et al., 2019). A widely used example, the OligoMM12, is a gnotobiotic consortium of 12 cultivable mouse-derived strains representing the major five bacterial phyla in the murine gut (Brugiroux et al., 2016). It is reproducible between facilities (Eberl et al., 2020) and extensive data now exists on the metabolism of individual species and their metabolic interactions with each other (Streidl et al., 2021; Weiss et al., 2021; Wotzka et al., 2019; Yilmaz et al., 2021). Understanding how, and to what extent, this gnotobiotic microbiota reconstitutes the metabolic phenotype of conventional mice is therefore of broad relevance for microbiota research.

52 Circadian variations in microbiota function adds an extra layer of complexity to metabolic
53 interactions between the host and the microbiota. Circadian feeding is a major driver of microbiota
54 composition (Thaiss et al., 2014; Zarrinpar et al., 2014). The luminal concentration of fermentation
55 products such as short-chain fatty acids (SCFA) shows a dramatic circadian oscillation linked both
56 to food intake and to intestinal motility (Tahara et al., 2018). Microbiota-derived molecules are
57 known to influence host nutrient absorption (Wang et al., 2017) and host metabolic gene
58 expression (Kuang et al., 2019; Thaiss et al., 2016). However, much of our current knowledge is
59 derived from indirect calorimetry measurements made over a time period shorter than 24h
60 (Bäckhed et al., 2004; Halatchev et al., 2019; Kübeck et al., 2016; Wostmann et al., 1968).
61 Measurements of the same host-microbiota system, if taken at different timepoints in the circadian
62 cycle of metabolism, could therefore be wrongly interpreted as qualitative shifts in microbiota
63 function. Consequently, to understand the influence of the microbiota on host energy metabolism,
64 it is key to quantify variation over the full circadian cycle.

65 A challenging aspect of addressing the influence of the OligoMM12 microbiota on host metabolism,
66 is that long-term experiments require hygiene barrier conditions similar to those required to work
67 with germ-free mice. In particular, standard metabolic cage systems do not permit maintenance
68 of an axenic environment and moving mice between the open cages typically used in isolator
69 systems where such animals are normally bred, to IVC-cage-like systems used for most metabolic
70 cages, can be associated with stress and behavioral abnormalities (Rabasa and Dickson, 2016).
71 We have therefore built an isolator-housed metabolic cage system. Based on the TSE
72 PhenoMaster® system, we can monitor levels of O_2, CO_2 and hydrogen every 24min for up to 8
73 cages, across two separate isolators in parallel, while maintaining a strict hygienic barrier. This
74 way, longitudinal monitoring of metabolism can be carried out over periods of several weeks in
75 germ-free and gnotobiotic mice.

76 In this study, we applied this system to understand how well gnotobiotic microbiota replicate the
77 influence of a complex microbiota on host metabolism. We compared the metabolic profile of
78 germ-free (GF), gnotobiotic (OligoMM12) and conventionally raised mice (specific-opportunistic-
79 pathogen free, SPF) fed *ad libitum* with standard chow, using isolator-based indirect calorimetry.
80 Similar to what has been described before (Krisko et al., 2020; Kübeck et al., 2016), we found no
81 significant differences in energy expenditure among GF and SPF mice. These results are in
82 contrast to other work (Bäckhed et al., 2004; Levenson et al., 1969; Li et al., 2019; Wostmann et
83 al., 1968), but the discrepancies can potentially be explained by the methods applied for
84 normalizing energy-expenditure data. Germ-free and gnotobiotic mice exhibit extensive water
85 retention in the cecal lumen which can contribute up to 10% of the total body weight. This water
86 is metabolically inert but is included in the mass used for normalization in reports where a
87 difference in energy expenditure is reported (Bäckhed et al., 2004; Levenson et al., 1969; Li et al.,
88 2019; Wostmann et al., 1968). When accounting for cecal inert mass, no significant difference in
89 energy expenditure can be found in either germ-free or the gnotobiotic OligoMM12 mouse line. By
90 calculating consumed calories in food and waste calories in feces, we could replicate earlier
91 findings that germ-free and gnotobiotic mice are less efficient at extracting calories from standard
92 mouse chow. However, our calculations demonstrated that this is well-compensated by increased
93 food intake such that all mice absorb a similar number of calories from food each day. Interestingly,
94 despite indistinguishable energy expenditure, and indistinguishable energy absorption from food
95 each day, OligoMM12 mice showed increased fat mass compared to both, germ-free and SPF
96 mice. Consistent with alterations in energy storage patterns, their circadian patterns of respiratory
97 exchange ratio (RER) and certain metabolites in liver and plasma, phenocopied SPF mice during
98 the dark phase, but germ-free mice during the light phase. Our study indicates that a
99 reductionist/synthetic microbiota can specifically recover microbiota function in the dark (active)
100 phase, but not in the light (resting/fasting) phase of the circadian cycle. This represents a valuable

101 tool for identifying critical microbiota species and functions needed to support healthy host
102 metabolism throughout the day.

103 **RESULTS**

104 In order to compare to published literature on germ-free and colonized mouse metabolism, we
105 compared male, adult age-matched (12-14wks old) germ-free (GF), gnotobiotic (OligoMM12) and
106 conventionally raised (SPF) mice, all bred and raised in flexible-film isolators and with a C57BL/6J
107 genetic background. Indirect calorimetry measurements were carried out in flexible-film surgical
108 isolators accommodating a TSE PhenoMaster® system (schematic view in Fig. 1A, picture Fig.
109 1B). Mice were adapted for between 24-36h to the single-housing condition inside isolator-based
110 metabolic chambers before data collection. Variations on O_2, CO_2 and hydrogen, along with food
111 and water consumption, were recorded every 24 min on each metabolic cage. We could confirm
112 that germ-free mice maintain their germ-free status over at least 10 days of accommodation in
113 these cages, via culture-dependent and culture-independent techniques (see Methods).

114 **Body composition in GF, OligoMM12 and SPF mice**

115 After 6-12 days of data recording mice were fasted for 4-5 hours and euthanized (approximately
116 at ZT6 ± 1 hour), and body mass and body composition were measured. As cecal mass (cecal
117 tissue plus its content) is affected by the colonization status (Wostmann et al., 1968), we first
118 assessed the cecal mass in GF, OligoMM12 and SPF and its impact on body mass. We found
119 that cecal mass was inversely correlated to the microbiota complexity, starting at approximately
120 0.5 g in SPF mice, increasing to around 1.5 g in OligoMM12 mice and reaching 3 g on average in
121 GF mice (Fig.1C). Note that this represents around 10% of total body mass in GF mice (Suppl.
122 Fig.1A), which translates into a trend to increased total body mass in GF mice (Fig, 1D). This trend
123 was completely reverted after removal of the cecum from total mass (Fig. 1E).

124 Measurements of body composition in mice are often performed using EchoMRI, which yields data
125 on lean, fat and water mass. As we observed that the cecum represented such a large and variable

126 fraction of body mass, we compared EchoMRI read-outs of “lean” and “fat” body mass before and
127 after removal of the cecum (Suppl. Fig.1B-G). We found a strong correlation between the total
128 lean mass measured by EchoMRI with and without the cecum (Suppl. Fig 1B) (Suppl. Fig.1C), i.e.,
129 cecum removal consistently reduced the lean mass readout by 5 to 10% (Suppl. Fig. 1D).
130 Therefore, cecum removal has a consistent effect on lean mass across groups. For ease of
131 comparison to published work, we decided to use lean mass obtained by EchoMRI *before*
132 *dissection* for definitive energy expenditure calculations. We observed a trend in lean body mass
133 with GF having a lower lean body mass than SPF mice, and OligoMM12 mice showing an
134 intermediate phenotype (Fig. 1F). However, we were underpowered to detect a significant
135 difference between groups, and we estimate that at least 22 mice per group would be needed to
136 achieve statistical significance by one-way ANOVA if the current group differences are real – a
137 number that was beyond the scope of the current study.

138 In contrast, EchoMRI fat mass measurements pre- and post-cecum dissection were poorly
139 correlated in GF mice (Suppl. Fig. 1E) attributable to a variable scoring of cecal content as fat or
140 water. In GF mice, cecum removal resulted in a decrease in EchoMRI fat mass readout of between
141 5 to 48% (Suppl. Fig. 1F) We also observed a shift towards *higher* fat mass readings in SPF mice
142 after cecum removal (Suppl. Fig. 1F and Suppl. Fig. 1G); further highlighting the need for caution
143 in interpreting EchoMRI readouts for fat mass in mice with major differences in intestinal
144 colonization. Therefore, we proceeded to directly weigh the fat depots accessible to dissection
145 (interscapular brown adipose tissue, iBAT; and, inguinal and visceral white adipose tissue, iWAT
146 and vWAT). There was no significant difference between GF and SPF mice in size of the explored
147 fat depots; however, OligoMM12 mice accumulated more fat in all explored depots than GF mice,
148 including more iBAT and vWAT compared to SPF mice (Fig 1G).

149 **Energy metabolism and energy balance in GF, OligoMM12 and SPF mice**

150 Body composition is determined by the quantity of calories absorbed from food, and whether these
151 calories are directly expended or are stored. Energy expenditure was estimated using VO_2 and
152 VCO_2 readouts (Meyer et al., 2015) and normalized as described before (Mina et al., 2018;
153 Speakman, 2013; Tschop et al., 2011) using EchoMRI lean body mass and dissected fat mass.

154 In contrast to some previous reports (Bäckhed et al., 2004; Levenson, 1978; Li et al., 2019;
155 Wostmann et al., 1968), but aligned with others (Krisko et al., 2020; Kübeck et al., 2016), we found
156 no significant difference in daily energy expenditure (Fig. 2A and Fig. 2B) or VO_2 (Suppl. Fig. 2A
157 and Suppl. Fig. 2B) between GF, OligoMM12 and SPF mice after normalization using a regression
158 model that included lean body mass and total dissected fat mass as predictive variables. This lack
159 of difference was also observed when light and dark phases were analyzed separately (Fig. 2B
160 and Suppl. Fig. 2B). “Classical” normalization procedures (dividing by mass) also showed no
161 difference between groups when lean body mass, or “total body mass after cecum dissection” was
162 used for normalization of energy expenditure (Fig. 2C and D) or VO_2 (Suppl. Fig. 2C and D).
163 Unsurprisingly, we did find a significant difference during the dark phase in energy expenditure
164 (Fig. 2E) and VO_2 (Suppl. Fig. 2E) between GF and SPF mice if “total body mass” (i.e., including
165 the large inert cecum mass in germ-free and gnotobiotic mice) was used for normalization.
166 Therefore, at least when comparing to the SPF microbiota used in this study, absence of a
167 microbiota does not result in altered daily energy expenditure in metabolically active tissues.

168 We next investigated increased calorie absorption from food by comparing the daily energy
169 ingestion from food and calorie excretion in feces of GF, OligoMM12 and SPF mice. The difference
170 between these two values estimates the absorbed calories. As reported previously (Wostmann et
171 al., 1983), GF animals ingested on average between 10-20% more standard chow compared to
172 OligoMM12 and SPF mice (Fig. 2F). Correspondingly, GF animals also excreted a much larger
173 dry mass of feces, while OligoMM12 mice produced an intermediate fecal mass and SPF mice
174 excreted the least (Fig. 2G).

175 Remarkably, energy density of dry feces was lower in GF mice (3.7 Kcal/g) compared to colonized
176 mice (OligoMM12 and SPF, 4.0 Kcal/g); with the latter showing no difference among them (Fig.
177 2H). This gap between GF and mice with microbiota can likely be explained by the fact that
178 although fecal bacteria improve energy release from food, a considerable fraction of that energy
179 remains stored in the bacteria present in the feces. Assuming certain averaged parameters (dry
180 mass of a bacterium = 2.26×10^{-13}g / bacteria cell (Dennis and Bremer, 2008), density of bacteria
181 in feces = 5×10^{11} bacteria cells / g of feces (Barlow et al., 2020), and energy stored in bacteria =
182 4.58 Kcal/g of dry bacteria mass (Popovic, 2019)); we estimated that the fecal microbiota of
183 colonized mice can contribute approx. 0.52 Kcal/g of dry fecal mass – slightly more than the energy
184 density difference between fecal energy density in colonized and germ-free mice.

185 We then used these values for food intake, fecal dry mass output, and fecal energy density to
186 estimate energy absorbed from the feces. We found that the higher food consumption in GF mice
187 (Fig. 2I) almost perfectly counterbalance their corresponding higher energy excretion in feces (Fig.
188 2J), such that all mice extract around 9 Kcal per day from their food (Fig. 2K). This is consistent
189 with our measurements of daily energy expenditure by indirect calorimetry (Fig. 2B), although it
190 fails to explain the observed adiposity in the OligoMM12 mice (Fig. 1G). Unexpectedly, the
191 OligoMM12 efficiency of release of calories from chow remains similar between germ-free and
192 OligoMM12 mice. Given that the gut content of both OligoMM12 and SPF mice is densely
193 colonized, and the fecal energy density is similar; it should be noted that the lower amount of
194 energy extracted by the OligoMM12 is not so much due to a poorer digestive capacity of the
195 gnotobiotic gut microbes, but rather that compared to the SPF microbiota, the calories extracted
196 by the OligoMM12 microbiota are either retained within the microbes or not converted into
197 compounds that can be taken up by their host (Fig. 2L).

198 We therefore concluded that daily energy expenditure and daily energy absorption from food vary
199 only within the range of experimental error intrinsic to indirect calorimetry experiments. At a

200 fundamental level, food intake therefore seems to be well regulated by microbiota-released
201 calories. Despite this, OligoMM12 mice have an elevated fat mass. It remains a distinct possibility
202 that gain of fat mass depends on the cumulative effect of very small differences in energy intake
203 and energy expenditure that are simply not resolvable in our system. An alternative explanation is
204 that microbiota composition influences energy storage. In order to gain a deeper insight into
205 underlying mechanisms we carried out a series of more detailed analyses of metabolism.

206 **Circadian changes in RER and microbiota-derived hydrogen and short-chain fatty acids**
207 **(SCFA)**

208 Respiratory exchange ratio (RER, the ratio of CO_2 produced per O_2 consumed) is widely used as
209 an informative proxy for substrate utilization (i.e., glucose or fatty acids) for oxidation in tissues.
210 We observed that GF mice have a lower RER compared to SPF mice in both light and dark phases,
211 indicative of increased fat/decreased glucose metabolism in GF mice (Fig 3A). These changes in
212 RER are not related to differences in feeding patterns as all mice have a similar food intake
213 patterns during the periods in which their RERs differ the most (Fig. 3B).

214 Differences in RER provided a clue that there could be differences in energy storage in mice with
215 different microbiota status. Microbial fermentation products, including short-chain fatty acids
216 (SCFA) and lactate, can be directly used as energy and carbon-sources by the murine host, and
217 are generated by the microbiota via processes that liberate molecular hydrogen. We therefore
218 quantified hepatic concentrations of glycogen, and cecal concentrations SCFA, at Zeitgeber 5
219 (ZT5, 5h into the light phase) and 16 (ZT16, 4h into the dark phase). Hydrogen was measured
220 continuously during the circadian cycle.

221 Hepatic glycogen levels show a circadian rhythm, which usually peaks early during the transition
222 between dark to light phase (ZT2-4), and drops to its minimum during the early hours of the dark

223 phase (ZT14-16) in nocturnal rodents (Doi et al., 2010; Ishikawa and Shimazu, 1976). We found
224 similar accumulation of hepatic glycogen in GF, OligoMM12 and SPF mice at ZT5; however, GF
225 and OligoMM12 mice drop to lower levels of hepatic glycogen compared to SPF mice at ZT16 (Fig
226 3C). This differential pattern in GF/OligoMM12 compared to SPF mice may indicate that, although
227 they can equally fill up hepatic glycogen storages at the end of the dark phase, GF and OligoMM12
228 show faster depletion of hepatic glycogen during the light phase.

229 Hydrogen, a byproduct of fiber fermentation by the microbiota, was also measured in the exhaust
230 air of the metabolic cages. We found a clear circadian pattern in hydrogen production between
231 OligoMM12 and SPF mice (Fig. 3D). Hydrogen levels in OligoMM12 and SPF mice decreased
232 down to the limit of blank (GF level as reference) during the light phase, to later peak after food
233 intake resumes during the dark phase. In addition, OligoMM12 mice showed a higher production
234 of hydrogen than SPF mice during the dark phase even after regression-based normalization by
235 cecal mass (Fig. 3D). Therefore, the higher dark phase hydrogen measurements in the
236 OligoMM12 mice are not just the result of a larger cecal mass, but of the OligoMM12 microbiota
237 producing hydrogen at a higher rate per cecal content mass than the SPF microbiota.

238 SCFA are the other major output of bacterial fermentation in the large intestine, as well as being
239 key bioactive compounds produced by the large intestinal microbiota. SPF mice showed the
240 highest cecal concentrations of acetate, butyrate, and propionate during both the light phase and
241 dark phase (Fig. 3E). Interestingly, OligoMM12 mice showed only 20-50% of the SCFA
242 concentrations observed in SPF mice but instead showed high production of lactate during the
243 dark phase (Fig. 3E). In germ-free mice, all analyzed metabolites had levels below the limit of
244 blank except for lactate, which could correspond to host-produced L-lactate (Zarrinpar et al., 2018)
245 (our assay is not able to differentiate the enantiomers). As the total mass of cecum content is
246 widely different among GF, OligoMM12 and SPF mice, we also estimated the total quantity of
247 each compound in the cecal content by multiplying the concentration (Fig. 3E) by the cecal mass

248 for each group (Fig. 1C) while propagating the uncertainty of each measurement, as a way of
249 representing the total availability of SCFA for the different hosts. This transformation has quite a
250 major impact on how these data can be interpreted: when taking cecal mass into account,
251 OligoMM12 mice have considerably higher levels of acetate during the light and dark phase and
252 of propionate during the dark phase than SPF mice, while butyrate levels remain low. There is
253 also an increased abundance of lactate and succinate in the OligoMM12 cecum content (Fig. 3F).
254 Although we cannot directly link these microbial metabolites to the phenotype of the OligoMM12
255 mice, this underlines the major differences in metabolite profiles in the large intestine when
256 comparing germ-free, gnotobiotic and SPF mice. High lactate production by the microbiome
257 certainly warrants further study for potential metabolic effects on the host.

258 **Circadian changes in liver and plasma metabolites in GF, OligoMM12 and SPF mice**

259 Finally, to increase our metabolic resolution, we applied UPLC-MS to perform untargeted
260 metabolomics in the liver and plasma during the light (Zeitgeber 5) and dark phase (Zeitgeber 16)
261 in GF, OligoMM12 and SPF mice. Principal component analysis (PCA, Fig. 4A and Fig. 4B)
262 separates the SPF, OligoMM12 and GF groups variably during light and dark phases. Correlating
263 to what we observed in the RER during the light phase, GF and OligoMM12 cluster closely and
264 are clearly separated from the SPF in the light phase PCA analysis for both liver (Fig. 4A) and
265 plasma samples (Fig. 4B). During the dark phase, although OligoMM12 mice begins to
266 differentiate from GF metabolome, it still does not recapitulate the metabolome of SPF mice either
267 in liver (Fig. 4A) or plasma samples (Fig. 4B).

268 We used the package MetaboAnalystR (Chong and Xia, 2018) to identify compounds that are
269 significantly different in pair comparisons between OligoMM12 mice and their GF and SPF
270 counterparts by untargeted peak extraction and map them into metabolic pathways using the
271 KEGG database. We found several pathways differentially enriched when OligoMM12 mice were

272 compared to GF or SPF counterparts during the light and dark phase in liver (Fig. 4C) and plasma
273 (Fig. 4D), including amino acid, bile acids, and fatty acid metabolism. Additionally, we selected
274 compounds that belong to these differentially enriched pathways or have been previously
275 identified to have circadian changes in obese patients (Nowak, 2021), confirmed their structure by
276 using chemical standards, and performed a targeted peak extraction for a more precise
277 comparison among groups (Suppl. Table 1). We observed that for certain metabolites the
278 OligoMM12 microbiota produce an intermediate phenotype between GF and SPF mice, e.g., a
279 subset of bile acids, in liver (Suppl. Fig 3A) and plasma (Suppl. Fig 3B).

280

281 **DISCUSSION**

282 Since the early days of nutritional studies, there has been a clear interest to understand the role
283 of microbiota in host morphology, physiology and nutrition (Gordon and Pesti, 1971; Levenson,
284 1978). Pioneering work comparing germ-free animals with conventionally raised or gnotobiotic
285 counterparts already described differences in food intake, energy extraction from diet and energy
286 expenditure by indirect calorimetry (Levenson et al., 1969; Wostmann et al., 1983). More recently,
287 researchers have explored the effect of specific microbiota communities and how they influence
288 energy metabolism and body composition in the host (Ridaura et al., 2013; Suárez-Zamorano et
289 al., 2015; Turnbaugh et al., 2006).

290 Here, by carefully checking the validity of different measurement types, we found no significant
291 difference in lean body mass among germ-free (GF), gnotobiotic (OligoMM12) and conventionally
292 raised (SPF) mice. Interestingly, there was a significant increase in fat depots in OligoMM12 mice
293 compared to GF and SPF animals. Previous studies diverged on the effect of microbiota on fat
294 mass accumulation during conventional/low-fat diet feeding; reporting either increased fat mass
295 in SPF mice (Bäckhed et al., 2004) or no difference compared to GF mice (Kübeck et al., 2016).
296 However, it should be noted that there can be huge differences between SPF microbiota within
297 and between animal facilities. GF mice transplanted with microbiota derived from obese donors
298 accumulated more fat mass compared to those transplanted with microbiota derived from lean
299 donors (Halatchev et al., 2019; Ridaura et al., 2013; Turnbaugh et al., 2006), with correlates
300 identified to individual species/strain abundance (Woting et al., 2014, 2015). SPF microbiota
301 matching more closely to those from obese donors could therefore be expected to give differing
302 results to ours. In contrast, minimal microbiota communities can be perfectly replicated across
303 sites, and can help to clarify the complex processes linking microbiota and host metabolism
304 (Becker et al., 2011). Further exploration of the metabolic effects of the OligoMM12 microbiota
305 community, and extended versions thereof, has potential to clarify if specific strains, species or

306 functional classes (Schmidt et al., 2018) are sufficient and necessary to drive the development of
307 increased fat depots in these mice.

308 Our analysis compared energy expenditure in GF, OligoMM12 and SPF mice and found no
309 significant difference among these mice. Normalization of mass-dependent variables by a per-
310 mass (or allometric transformation) ratio has been recognized as a common source of controversy
311 (Packard and Boardman, 1999; Tanner, 1949; White and Seymour, 2005), especially with large
312 changes in body mass composition (Butler and Kozak, 2010; Kaiyala and Schwartz, 2011), and
313 there have been several publications calling for the use of better statistical methods (Arch et al.,
314 2006; Fernández-Verdejo et al., 2019; Tschop et al., 2011). We found that, when the cecal content
315 mass is very different among groups, using total body mass for normalization introduces a
316 considerable bias in normalized energy expenditure estimation. Interestingly, it was long-ago
317 observed that surgical removal of the cecum equalized the oxygen consumption between germ-
318 free and conventional rats; as well as other measurements normalized by total body mass
319 (Wostmann et al., 1968). With normalization using linear regression models based on lean-mass
320 and fat-mass (Mina et al., 2018), we and others found no significant differences in energy
321 expenditure by indirect calorimetry between GF and SPF mice under standard chow diet
322 conditions (Krisko et al., 2020; Kübeck et al., 2016; Li et al., 2021). Importantly, we suggest
323 cautious interpretation of lean and fat mass readouts obtained by EchoMRI when comparing mice
324 with major differences in intestinal content composition. We are also keen to point out the more
325 general limitations of our observations: only one gnotobiotic microbiota and one SPF microbiota
326 were analyzed, and our conclusions pertain exclusively to these. We in no way exclude the
327 possibility that some microbiota constituents or conformations *can* influence host energy
328 expenditure (Halatchev et al., 2019) and/or body composition (Ridaura et al., 2013; von
329 Schwartzenberg et al., 2021; Turnbaugh et al., 2006). In addition, it should be noted that indirect

330 calorimetry is an inherently noisy data type, and small differences in daily energy expenditure are
331 impossible to resolve via this technique (Corrigan et al., 2020; Fernández-Verdejo et al., 2019).

332 Nevertheless, the lack of measurable difference in energy expenditure between GF, OligoMM12
333 and SPF mice is aligned with our finding that the amount of energy obtained by *ad libitum* food
334 intake was also remarkably similar among the groups. GF mice seem to accurately compensate
335 the lower capacity of energy extraction from diet by increasing food intake. While this seems
336 generally to be in agreement with models that described the regulation of appetite (and therefore
337 energy intake) by the basal energy requirement of the individual (MacLean et al., 2017; Stubbs et
338 al., 2018), it remains surprising given the discrepancy in the types of substrates available for
339 oxidative metabolism in colonized and germ-free mice, revealed by RER differences. Although
340 germ-free mice have a longer total gastrointestinal transit time than SPF mice (Touw et al., 2017),
341 very little calorie absorption from food can occur after ingested food reaches the cecum of a germ-
342 free mouse, whilst an SPF mouse will release usable energy from their food via microbial
343 fermentation for several more hours in the cecum and colon, generating a major time-difference
344 in the absorption of calories after eating in germ-free and SPF animals. This compensation seems
345 also to function in mice colonized with the OligoMM12 microbiota, where despite robust microbial
346 fermentation (read out as hydrogen and fermentation product production) and identical fecal
347 energy density to SPF mice, energy recovery from ingested food is poor due to the volume of
348 feces shed. A clear conclusion from these observations is that microbiota-dependent changes in
349 metabolic substrates, and timing of calorie absorption, are well integrated in the murine central
350 regulation of appetite over the course of a day (Fetissov, 2017).

351 Despite this broadly successful regulation of food intake and energy expenditure, at the molecular
352 level, major differences were observed between the mice with different microbiota. First,
353 OligoMM12 mice displayed an RER at the GF level during the light phase (when mice typically
354 sleep and fast) but raised up to SPF levels during the dark phase (i.e., when mice are active and

355 eating). It therefore appears that the OligoMM12 microbiota better recapitulates the microbiome
356 effects on the host energy substrate use during the dark (active) phase when food-derived
357 carbohydrates are abundant in the large intestine, but not in the light (sleeping) phase when mainly
358 host-derived carbon sources are available in the large intestine. This potentially correlates with
359 the SCFA concentrations observed in the cecum content of the OligoMM12, which was associated
360 with a predominance of succinate and lactate, at the expense of propionate and butyrate. In
361 complex microbiotas, lactate is typically further metabolized to butyrate by specific firmicutes
362 (Belenguer et al., 2011; Duncan et al., 2004; Flint et al., 2015), which may be lacking or
363 insufficiently abundant in the OligoMM12 mice. As lactate can inhibit lipolysis in adipocytes (Cai
364 et al., 2008; Liu et al., 2009), this raises an interesting theme for follow-up studies to define the
365 role of microbiota-derived lactate in host metabolism. In line with the RER data, we also observed
366 that the liver and plasma metabolite profiles of OligoMM12 mice clustered closer to GF mice than
367 to SPF mice. In addition, certain aminoacids were differentially represented between OligoMM12
368 and GF or SPF mice, as it has been described before (Claus et al., 2008; Mardinoglu et al., 2015).
369 Interestingly, OligoMM12 had a bile acid profile closer to GF than SPF mice, for example showing
370 GF-levels of hepatic β-murocholic acid and taurine- β-murocholic acid, the predominant bile acid
371 in the liver of GF mice (Sayin et al., 2013). Follow up studies with manipulation of the OligoMM12
372 microbiota or metabolic interventions are a promising tool to pull apart the circadian effects on
373 RER, the influence of an unusual fermentation product profile, and other more subtle metabolic
374 changes on overall metabolic health of the murine host.

375 In conclusion, our study showed that isolator-based indirect calorimetry is possible and allows
376 detailed analysis of the metabolism of germ-free and gnotobiotic mice in real-time. Data generated
377 with this system demonstrated that microbiota-released calories are well integrated in host energy
378 balance, and that daily energy expenditure was not significantly influenced by microbiota
379 composition in our mice. Nevertheless, mice colonized with the OligoMM12 gnotobiotic microbiota

380 accumulated more fat mass and display a GF-like RER during the light phase but an SPF-like
381 RER during the dark phase, indicative of altered metabolic substrate usage and energy storage.
382 Correspondingly, the liver metabolome of mice colonized with the OligoMM12 showed alterations
383 in bile acid, fatty acid and amino acid metabolism and tended to cluster with the GF liver
384 metabolome during the light-phase, and with the SPF liver metabolome during the dark phase.
385 This reveals the potential for gnotobiotic microbiota communities to investigate the mechanisms
386 underlying the influence of microbiota on host metabolic health. As microbial dysbiosis is
387 associated with a range of human diseases, circadian analysis of energy balance represents a
388 crucial tool in the mining of microbiome data for therapeutic and diagnostic purposes.

ACKNOWLEDGEMENTS

We would like to thanks to Sven Nowok, Thomas Fehr, Andre Galhano and Susanne Freedrich for their support in the establishment of the gnotobiotic metabolic phenotype facility in the ETH Phenomic Center. Also, we thank Maria L. Balmer for her comments and suggestions for the manuscript. The gnotobiotic metabolic phenotype facility was initially funded by the FreeNovation grant (Novartis). E.S. and W-D.H. are supported by the NCCR Microbiomes, a research consortium financed by the SNF. E.S. acknowledges the support of the Swiss National Science Foundation (40B2-0_180953, 310030_185128), European Research Council Consolidator Grant, and Gebert Rüf Microbials (GR073_17) and the Botnar Research Centre for Child Health Multi-Invesitigator Project 2020. This project is part of "Zurich Exhalomics", a flagship project of “Hochschulmedizin Zürich”.

Author Contributions

Conceptualization, D.H., W-D.H., C.W. and E.S.; Methodology, D.H., J.L., W.S., R.Z. C.W. and E.S.; Formal Analysis, D.H., J.L, W.S., T.G. and M.A.; Investigation, D.H., J.L., W.S. and S.N.; Resources, B.S., R.Z., W-D.H., C.W. and E.S.; Writing – Original draft, D.H. and E.S.; Writing – Review and Editing D.H., J.L., W.S, T.G, M.A, S.N., A.J.M., B.S., R.Z., W-D.H., C.W and E.S.; Visualization, D.H., W-D.H., C.W. and E.S.; Supervision, W-D.H., C.W. and E.S.; Funding acquisition, W-D.H., C.W., A.J.M, and E.S.

Declaration of Interest

The authors declare no competing interests.

409 **METHODS**

410 **Animals**

411 We used C57B6/J male mice aged between 12-14 weeks. We compare germ-free mice (GF), with
412 a 12-strain gnotobiotic microbiota (Brugiroux et al., 2016) (OligoMM12) and specific-pathogen free
413 mice (SPF). GF and OligoMM12 mouse lines are bred and maintained in open-top cages within
414 flexible-film isolators, supplied with HEPA-filtered air, and autoclaved food and water ad libitum.
415 As we are aware that housing conditions may influence behavior and potentially metabolism, we
416 also bred and maintained a SPF colony under identical conditions inside a flexible-film isolator
417 specifically for this study, such that all mice experienced identical living conditions, food, and water.
418 Mice were adapted for between 24-36h after transfer from the breeding isolators to the isolator-
419 based metabolic chambers. For long term experiments, mice were periodically re-housed in
420 couples for short periods of times to avoid stress of extended single-housing conditions. In all
421 cases, animals were maintained with standard chow (diet 3807, Kliba-Nafag, Switzerland) and
422 autoclaved water. Germ-free status was confirmed at the end of the long-term experiments by
423 culturing cecal content in sterile BHIS media in aerobic and anaerobic conditions for a week. In
424 addition, cecal content was frozen at -20°C for a week, then stained with SYBR Gold and assessed
425 by bacterial flow cytometry (Moor et al., 2016) using similarly processed SPF mice cecal content
426 as positive control for the presence of bacteria. All experiments were conducted in accordance
427 with the ethical permission of the Zürich Cantonal Authority.

428 **Indirect calorimetry**

429 The isolator-housed TSE PhenoMaster® system allows instantaneous measurements of oxygen,
430 carbon dioxide and hydrogen levels as well as total feed and water consumption while keeping a
431 strict hygiene level of control. The metabolic isolator system consists of an adapted set of two

432 flexible-film surgical isolators, each of them housing four metabolic cages from the TSE
433 PhenoMaster® system (TSE Systems, Germany). Room air is pulled into the isolator by a vacuum
434 pump passing through a double set of HEPA filters. Then, each cage is connected via a second
435 HEPA filter through the back wall of the isolator to the CaloSys setup, which pulls sterile air from
436 the isolator into the cages using negative pressure. Air coming from the cages is dehumidified at
437 4°C and sequentially passed by a Sensepoint XCD Hydrogen gas analyzer (Honeywell Analytics,
438 Hegnau, Switzerland) and standard oxygen and carbon dioxide censors provided in the TSE
439 PhenoMaster® system. A two-point calibration of all analyzers using reference gases was
440 performed within 24 h before each animal experiment. Data was recorded using a customized
441 version of the TSE PhenoMaster® software modified to integrate hydrogen measurements.

442 For indirect calorimetry measurements, the animals were transported in pre-autoclaved, sealed
443 transport cages from the breeding isolators into the metabolic isolator system. Mice were single
444 housed and adapted for between 24-36h before starting recording measurements to ensure
445 proper access to food and water as well as account for initial exploratory behavior. Mice were kept
446 up to 10 days at a stable temperature (21-22°C) with *ad libitum* availability of standard chow and
447 water. The days were divided into a dark and light period of 12 hours each. In this study, we kept
448 the air flow of 0.4 L/min and recorded individual cage data (gases production and food/water
449 consumption) every 24min (time set per cage for measurement stabilization 2.5min). In long
450 experiments, mice were periodically pair-housed for 24h to prevent stress due to prolonged single
451 housing.

452 **Body composition measurements**

453 At the end of the experiment, mice were fasted for 4 hours (Zeitgeber 1 till 5) before for body
454 composition measurements. We used magnetic-resonance whole-body composition analyzer
455 (EchoMRI, Houston, USA) to analyze mice body composition (lean and fat mass). Then, mice

456 were euthanized using CO_2 according to approved protocols. Total body mass was obtained by
457 weighing the full carcass and cecum was dissected and weighed by one investigator (DH). For a
458 set of mice, we remeasured body composition by EchoMRI after cecum removal. Finally, fat
459 depots were dissected from all mice by one investigator (W.S.) that was blinded to the hygiene
460 status of the mice. Interscapular brown adipose tissue (iBAT), inguinal white adipose tissue (iWAT)
461 and visceral white adipose tissue (vWAT) were sampled and weighted.

462 **Food intake, fecal samples and bomb calorimetry**

463 Daily food intake was obtained as the mean value of food intake recorded by the TSE
464 PhenoMaster® system during the course of the experiment. In addition to the mice reported in the
465 indirect calorimetry experiments, we also collected food intake data from a set of selected
466 experiments in which we collected fecal pellets produced during 24h. For daily fecal excretion
467 measurements, we cleaned up the bedding in the cage and replaced it for a clean and reduced
468 amount of bedding. After 24h, we collected the mix of bedding and fecal pellets. Fecal pellets were
469 manually collected from the bedding, transferred to 15ml tubes and stored at -20°C until bomb
470 calorimetry. Before bomb calorimetry, fecal samples were freeze dried in a lyophilizer overnight
471 (ALPHA 2-4 LDplus, Christ, Germany) and dry mass recorded. We used a C1 static jacket oxygen
472 bomb calorimeter (IKA, Germany) to quantify the residual energy present in these dry fecal pellets,
473 using approximately 0.2-0.5g of material. Energy content was normalized to grams of dry fecal
474 pellets.

475 **Metabolomics by UPLC/MS**

476 *Sample obtention and preparation*

477 Approximately at Zeitgeber 5 and 16, three mice of each group were euthanized, and liver and
478 plasma samples collected. To minimize variations among mice, individual mice were euthanized
479 with CO_2 and sampled as fast as possible. Blood was obtained by cardiac puncture, collected in
480 lithium heparin coated tubes, and kept on ice for further processing. Mice were perfused with PBS
481 and liver samples were obtained by dissection of the lower right lobe, collected on an 2ml
482 Eppendorf tube and flash frozen in liquid nitrogen. Finally, between 60-80 mg of cecal content was
483 collected in a 2ml Eppendorf tube and flash frozen in liquid nitrogen. After samples all samples
484 were obtained, blood samples were centrifuged 8000rcf for 5min, supernatant collected, and flash
485 frozen in liquid nitrogen. Samples were kept at -80°C until preparation for UPLC/MS.

486 *Short chain fatty acid quantification by UPLC/MS*

487 Samples were first homogenized in 70%-isopropanol (1 mL per 10 mg sample), centrifuged.
488 Supernatants were used for SCFA quantification using a protocol similar to previously described
489 (Liebisch et al., 2019). Briefly, a 7-points calibration curve was prepared. Calibrators and samples
490 were spiked with mixture of isotope-labeled internal standards, derivatized to 3-
491 nitrophenylhydrazones, and the derivatization reaction was quenched by mixing with 0.1% formic
492 acid. Four µL of the reaction mixture was then injected into a UPLC-MS system, [M-H]- peaks of
493 the derivatized SCFAs were fragmented and characteristic MS2 peaks were used for
494 quantification.

495 *Untargeted UPLC/MS*

496 Samples were thawed on ice. Serum samples were diluted with 90% methanol in water with a
497 volumetric ratio of 1:7, incubated for 10 min on ice for allowing protein to precipitate. Liver samples
498 were mixed with 75% methanol in water (2 mL/ 100 mg liver), homogenized using a TissueLyser
499 (Qiagen, Germany) at 25 Hz for 5 min. The result mixtures were centrifuged at 15,800 g, 4 °C for

500 15 min. 100 µL of the supernatants were filtered with 0.2 µm reversed cellulose membrane filter
501 and transferred to sample vials and used for UPLC/MS analysis with an ACQUITY UPLC BEH
502 AMIDE column (1.7 µm, 2.1 × 150 mm, Waters). Another 400 µL of the supernatants were then
503 lyophilized and resuspended in 80 µL 5% methanol in water, sonicated, filtered, and used for
504 UPLC/MS analysis with an ACQUITY UPLC BEH C18 column (1.7 µm, 2.1 × 150 mm, Waters,
505 RP column).

506 An ACQUITY UPLC system (I-Class, Waters, MA, USA) coupled with an Orbitrap Q-Exactive Plus
507 mass spectrometer (Thermo Scientific, San Jose, CA) were used for UPLC/MS analysis. For the
508 AMIDE column a flow rate of 400 µL/min was used with a binary mixture of solvent A (water with
509 0.1% formic acid) and solvent B (acetonitrile with 0.1% formic acid). The gradient starts from 1%
510 of A, then gradually increases to 70% of A within 7 min. Then a 1% of A is kept for 3 min. The
511 column was kept at 45 °C and the autosampler at 5° C.

512 For the RP column, the flow rate was set to 240 µL/min using a binary mixture of solvent A (water
513 with 5 % methanol and 0.1 % formic acid) and solvent B (methanol with 0.1 % formic acid). The
514 gradient starts from 95% of A, then gradually decreases to 5% of A within 10 min. A 100% solvent
515 of B is kept for 2 min, then a 100% of A is kept for 2min to restore the gradient. The column was
516 kept at 30 °C and the autosampler at 5 °C.

517 The MS was operated at a resolution of 140,000 at m/z = 200, with automatic gain control target
518 of $2x10^5$ and maximum injection time was set to 100ms. The range of detection was set to m/z 50
519 to 750. Untargeted MS data was extracted from raw MS files by using XCMS (Smith et al., 2006)
520 in R (v3.6.1), and then subject to pathway enrichment by using MetaboAnalystR (Chong and Xia,
521 2018).

522 *Compound identification and targeted peak extraction*

523 Chemical standards of selected compounds were diluted to 10 µg/mL and were analyzed using
524 the UPLC/MS methods described before. Identification was done by comparing retention time and
525 MS2 in liver/plasma samples with the chemical standards (Nowak, 2021). After confirming the
526 chemical identities of the compounds, targeted peak extraction was done using Skyline (v21.1)
527 (Adams et al., 2020).

528 **Data Analysis**

529 *Data quality control*

530 To facilitate analysis across different experimental runs, all times were converted into Zeitgeber
531 time (ZT; [h]), where 0-12 represents the light phase and 12-24 represents the dark phase. Any
532 datapoint taken before the start of the first occurrence of ZT=0 was discarded. To account for
533 faulty measurements caused by measurement imprecision, equipment malfunction or other
534 disruptive events, datapoints were removed from the raw datasets according to criteria based on
535 statistical and biological arguments. Food consumption values of 0.01 g during the 24min intervals
536 were considered as measurement noise and discarded. Negative values for food and water
537 consumption, as well as oxygen (dO_2) and carbon dioxide (dCO_2) differentials between the
538 measurement chambers and the reference chamber were also considered as measurement noise
539 and discarded. For the remaining subsets of measurements from the individual mice, we cleaned
540 up outlier measurements in food and water intake by eliminating values greater than 75th percentile
541 + 1.5 times interquartile range. Potential sources for outlier measurements in food and water
542 consumption observed included leaky water bottles and loss of food pellets during mice husbandry
543 procedures. A similar approach was used to eliminate outliers from dO_2 and dCO_2 values below
544 25th percentile - 1.5 times interquartile range. Potential sources for outlier measurements in gas
545 differentials included inappropriate sealing of individual metabolic cages or clogging of pre-
546 analyzer filters. Oxygen consumption (VO_2) and CO_2 production (VCO_2) was calculated using dO_2

547 and dCO_2 and the Haldane transformation as described before (Arch et al., 2006). Energy
548 expenditure was estimated from dO_2 and dCO_2 using Weir's approximation (Weir, 1949). As one
549 of the study objectives is to explore circadian patterns, if more than 20% of datapoints had to be
550 removed from a particular day for a particular mouse, all other datapoints from that subset were
551 discarded as well. After the cleanup process described above, the data from all different
552 experiment runs were pooled together for further analysis. The above processes lead to a
553 reduction in dataset size from 10472 to 9453 entries.

554 *Statistical analysis*

555 From the resulting dataset, energy expenditure over a certain period was calculated as the area
556 under the curve (trapezoid interpolation) of instantaneous values obtained during the 24min
557 measurements intervals. Food intake values calculated over a certain time are always cumulative.
558 To compare different mice in the above variables, variations in body mass and composition
559 between individuals need to be accounted for. As suggested in several publications (Fernández-
560 Verdejo et al., 2019; Speakman, 2013; Tschop et al., 2011), this was done by regression-based
561 analysis of covariance (ANCOVA). As such, a linear regression is performed on energy
562 expenditure as a function of lean body mass and fat depots mass, with the microbiota group as a
563 qualitative covariate. Then, each individual value is replaced by the sum of the corresponding
564 residual and the energy expenditure predicted by the linear model using the average lean body
565 and fat depot mass (calculated over all groups). Hydrogen production (difference in hydrogen
566 concentration between the measurement chambers and the reference chamber) was adjusted in
567 analogous fashion, using cecal mass (as a proxy for total gut microbiota mass) as a predictor.

568 For variables where the continuous evolution during the circadian cycle is of interest (RER, gross
569 hydrogen production), values were averaged at each time point for each individual. A generalized

570 additive model was used to fit a smooth line to these averages using a cubic penalized regression
571 spline (using R function mgcv::gam with formula y ~ s(x; bs = “cs”)).

572 For estimating derived variables (i.e., daily energy excretion) we used the R package “errors”
573 (Ucar et al., 2019). This package links uncertainty metadata to quantity values (i.e., mean “daily
574 fecal dry mass excretion”, mean “fecal energy content”) and this uncertainty is automatically
575 propagated when calculating derived variables (i.e., “daily energy excretion” = “daily fecal dry
576 mass excretion” x “fecal energy content”). Uncertainty is treated as coming from Gaussian and
577 linear sources and propagates them using the first-order Taylor series method for propagation of
578 uncertainty.

579 Hierarchical clustering and heatmap visualization were produced using the R package “pheatmap”
580 using Pearson correlation as distance measure for clustering and Ward's minimum variance
581 method using an algorithm that includes Ward’s criterion (Murtagh and Legendre, 2014). For the
582 Principal Component Analysis, we used the *prcomp* function which is present in built-in R stats
583 and the R package “factoextra” for visualization.

584 All group comparisons were analyzed by ANOVA and Tukey's honest significance test. For
585 comparisons of metabolites identified by targeted peak extraction among groups, area values
586 were log2 transformed before the statistical test.

587 **Resource availability**

588 *Lead contact*

589 Any further communication, including those related to resource sharing, may be directed to and
590 fulfilled by the lead contact Emma Slack (emma.slack@hest.ethz.ch).

591 *Materials availability*

592 This study did not generate new unique reagents.

593 *Data and code availability*

594 Source data for Fig. 1, 2 and 3, and Suppl. Fig. 1 and 2 are available in the Supplementary
595 Information. Source data for Fig. 4 and Suppl. Fig. 3 and the datasets and code used for all figures
596 in this publication are made available in a curated data archive at ETH
597 Zurich (https://www.research-collection.ethz.ch/handle/20.500.11850/501168) under the DOI
598 https://doi.org/10.3929/ethz-b-000501168.

599 **FIGURES TITLES AND LEGENDS**

600 **Figure 1: OligoMM12 mice have increase fat mass compared to GF mice and SPF C57B6/J**
601 **mice.** (A) Schematic representation of isolator-based indirect calorimetry system, with a TSE
602 PhenoMaster® calorimeter connected to two flexible surgical isolators with four metabolic cages
603 each. (B) Pictures of isolator-based indirect calorimetry system inside the facility. (C) Cecal mass
604 (tissue including luminal content). (D) Total body mass at the end of the experiment and before
605 cecum removal. (E) Total body mass after cecum removal. (F) Lean body mass acquired by
606 EchoMRI before cecum removal (N of mice per group with EchoMRI and indirect calorimetry
607 measurements: GF = 12, OligoMM12 = 8, SPF = 11). (G) Fat mass from interscapular brown
608 adipose tissue (iBAT), inguinal white adipose tissue (iWAT) and visceral white adipose tissue
609 (vWAT). Number of mice per group in all figures unless otherwise specified: GF = 16, OligoMM12
610 = 12, SPF = 11. p-values obtained by Tukey's honest significance test.

611 **Figure 2: Energy metabolism in GF, OligoMM12 and SPF C57B6/J mice.** (A) Linear regression
612 of energy expenditure and lean body mass based on EchoMRI during light and dark phase. Each
613 colored vertical line represents energy expenditure measurements during the experiment for one
614 mouse. (B) Energy expenditure during 24h period, or during the 12h light or dark phase. Values
615 represent area-under-curve normalized by regression-based analysis using lean body mass
616 obtained by EchoMRI and dissected fat mass. (C, D, E) Energy expenditure values obtained by
617 “classical” ratio-based normalization methods (dividing energy expenditure values per phase by
618 mass). (C) Area-under-curve after normalization by total mass after cecal dissection. (D) Area-
619 under-curve after normalization by lean body mass (EchoMRI). (E) Area-under-curve after
620 normalization by total body mass before cecal dissection. (F) Average daily food intake per mouse.
621 Mice represented in this figure include those that underwent long-term indirect calorimetry (Fig. 3)
622 and mice that only contribute to daily fecal pellet quantification/bomb calorimetry. (N of mice per
623 group: GF = 24, OligoMM12 = 19, SPF = 10) (G) Dry fecal output per mouse collected during a

624 24h period. (N of mice per group: GF = 12, OligoMM12 = 8, SPF = 4) (H) Energy content of dry
625 fecal output by bomb calorimetry. (N of mice per group: GF = 21, OligoMM12 = 11, SPF = 11). (I,
626 J, K, L) Estimation energy metabolism parameters. Number represented estimate mean value ±
627 1.96*combined standard uncertainty from measurements used for calculations. (I) Estimated daily
628 energy input (food intake* 3.94 Kcal/g). (J) Estimated daily energy excretion (daily fecal dry
629 mass*fecal energy content). (K) Estimated daily energy extraction (daily energy input – daily
630 energy excretion). (L) Estimated energy extraction from food as percentage of energy input ((daily
631 energy input - daily energy excretion)/daily energy input*100). Note that calculations in L, N and
632 M are per mouse and are not normalized to body mass. Number of mice per group in all figures
633 unless otherwise specified: GF = 9, OligoMM12 = 8, SPF = 10. p-values obtained by Tukey's
634 honest significance test.

635 **Figure 3: Circadian changes in Respiratory Exchange Ratio (RER), microbiota-derived**
636 **hydrogen and short-chain fatty acids (SCFAs).** (A) Comparison of circadian changes in RER
637 among GF, OligoMM12 and SPF C57B6/J mice. RER curves obtained by smoothing function of
638 data obtained every 24min per mouse over 10 days. Mean RER during the light phase (Zeitgeber
639 0-12) and dark phase (Zeitgeber 12-24). (B) Cumulative food intake during described ZT periods.
640 Mice included in this analysis are those that underwent long-term indirect calorimetry, and they
641 are a subset of the mice represented in Fig. 2F (C) Hepatic glycogen and triglyceride concentration
642 in samples obtained at Zeitgeber 5 and 16 (N=3 per group). (D) Hydrogen production, curves
643 obtained by smoothing function of data obtained every 24min per mouse. Area-under-curve after
644 regression-based normalization by cecal mass during the light and dark phase (N of mice per
645 group: OligoMM12 = 11, SPF = 10). (E) Concentration of short-chain fatty acids (acetate, butyrate,
646 propionate) and intermediate metabolites (lactate, succinate) products in cecal content. Number
647 of mice per group ZT5: GF = 4, OligoMM12 = 7, SPF = 7; ZT16: GF = 5, OligoMM12 = 7, SPF =
648 7. (F) Estimation total amount of short-chain fatty acids and intermediate metabolites by

649 multiplying measured concentration values by the cecal mass of the group. Number represented
650 estimate mean value ± combined standard uncertainty from measurements used for calculations.
651 Number of mice per group in all figures unless otherwise specified: GF = 13, OligoMM12 = 12,
652 SPF = 10. p-values obtained by Tukey's honest significance test.

653 **Figure 4. Metabolic profile comparison of GF, OligoMM12 and SPF C57B6/J mice by**
654 **UPLC/MS**. (A and B) Principal component analysis of metabolites identified by untargeted
655 UPLC/MS during the light phase (Zeitgeber 5) and dark phase (Zeitgeber 16) in (A) liver and (B)
656 plasma. (C and D) Metabolic pathways identified in the KEGG PATHWAY database; red dots
657 represent pathways containing compounds differentially enriched in (*top*) OligoMM12 vs. GF and
658 (*bottom*) OligoMM12 vs. SPF comparisons. Samples obtained during the light phase (Zeitgeber
659 5) and dark phase (Zeitgeber 16) in (C) liver and (D) plasma. Number of mice per group: Liver
660 ZT5: GF = 4, OligoMM12 = 6, SPF = 7; ZT16: GF = 4, OligoMM12 = 6, SPF = 7 / Plasma: ZT5:
661 GF = 4, OligoMM12 = 7, SPF = 7; ZT16: GF = 5, OligoMM12 = 6, SPF = 6.

662 **SUPPLEMENTAL INFORMATION TITLES AND LEGENDS**

663 **Supplementary Figure 1: Cecal mass interferes with fat mass estimation by EchoMRI.** (A)
664 Cecal mass (tissue including luminal content) as percentage of total body mass (N of mice per
665 group: GF = 16, OligoMM12 = 12, SPF = 11) (B) Lean body mass estimated by EchoMRI with and
666 without cecum. Equations show simple linear regression for estimating lean mass without cecum
667 based on lean mass with cecum; in brackets adjusted-R squared. (C) Lean mass variation after
668 cecum removal. (D) Lean mass variation after cecum removal as percentage of lean mass before
669 cecum removal. (E) Fat body mass estimated by EchoMRI with and without cecum. Equations
670 show simple linear regression for estimating fat mass without cecum based on fat mass with
671 cecum; in brackets adjusted-R squared. (F) Fat mass variation after cecum removal. (G) Fat mass
672 variation after cecum removal as percentage of lean mass before cecum removal. Number of mice
673 per group in all figures unless otherwise specified: GF = 13, OligoMM12 = 11, SPF = 15. p-values
674 obtained by Tukey's honest significance test.

675 **Supplementary Figure 2: Cecal mass interferes with normalization of VO_2.** (A) Linear
676 regression of VO_2 and lean body mass (EchoMRI) during light and dark phase. Each colored
677 vertical line represents energy expenditure measurements during the experiment per mouse. (B)
678 VO_2 during 24h period, or during the 12h light or dark phase. Values represent area-under-curve
679 normalized by regression-based analysis using lean body mass obtained by EchoMRI and
680 dissected fat mass (C, D, E) VO_2 values obtained by “classical” ratio-based normalization methods
681 (dividing energy expenditure values per phase by mass). (C) Area-under-curve after normalization
682 by total mass after cecal dissection. (D) Area-under-curve after normalization by lean body mass.
683 (E) Area-under-curve after normalization by total body mass before cecal dissection. Number of
684 mice per group in all figures unless otherwise specified: GF = 9, OligoMM12 = 8, SPF = 10. p-
685 values obtained by Tukey's honest significance test.

686 **Supplementary Figure 3. Metabolic profile comparison of GF, OligoMM12 and SPF C57B6/J**
687 **mice by UPLC/MS.** (A and B) Manually-curated list of compounds obtained by targeted peak
688 extraction from differentially expressed pathways in (A) liver and (B) plasma samples. p-values
689 obtained by Tukey's honest significance test after log2 transformation of area value. Number of
690 mice per group: Liver ZT5: GF = 4, OligoMM12 = 6, SPF = 7; ZT16: GF = 4, OligoMM12 = 6, SPF
691 = 7 / Plasma: ZT5: GF = 4, OligoMM12 = 7, SPF = 7; ZT16: GF = 5, OligoMM12 = 6, SPF = 6.

692 **Supplementary Table 1. List of metabolites identified by targeted peak extraction in the**
693 **UPLC/MS data**. Table indicates compound name, KEGG Entry number, type of column was
694 used for UPLC and if the peak matched the retention time and MS2 spectra identified with the
695 chemical standard in liver and plasma samples.

REFERENCES

Adams, K.J., Pratt, B., Bose, N., Dubois, L.G., St John-Williams, L., Perrott, K.M., Ky, K., Kapahi, P., Sharma, V., MacCoss, M.J., et al. (2020). Skyline for Small Molecules: A Unifying Software Package for Quantitative Metabolomics. J. Proteome Res. *19*, 1447–1458, 10.1021/acs.jproteome.9b00640.

Arch, J.R.S., Hislop, D., Wang, S.J.Y., and Speakman, J.R. (2006). Some mathematical and technical issues in the measurement and interpretation of open-circuit indirect calorimetry in small animals. Int. J. Obes. (Lond). *30*, 1322–1331, 10.1038/sj.ijo.0803280.

Bäckhed, F., Ding, H., Wang, T., Hooper, L. V, Koh, G.Y., Nagy, A., Semenkovich, C.F., and Gordon, J.I. (2004). The gut microbiota as an environmental factor that regulates fat storage. Proc. Natl. Acad. Sci. U. S. A. *101*, 15718–15723, 10.1073/pnas.0407076101.

Bäckhed, F., Manchester, J.K., Semenkovich, C.F., and Gordon, J.I. (2007). Mechanisms underlying the resistance to diet-induced obesity in germ-free mice. Proc. Natl. Acad. Sci. U. S. A. *104*, 979–984, 10.1073/pnas.0605374104.

Barlow, J.T., Bogatyrev, S.R., and Ismagilov, R.F. (2020). A quantitative sequencing framework for absolute abundance measurements of mucosal and lumenal microbial communities. Nat. Commun. *11*, 1–13, 10.1038/s41467-020-16224-6.

Becker, N., Kunath, J., Loh, G., and Blaut, M. (2011). Human intestinal microbiota: Characterization of a simplified and stable gnotobiotic rat model. Gut Microbes *2*, 25–33, 10.4161/gmic.2.1.14651.

Belenguer, A., Holtrop, G., Duncan, S.H., Anderson, S.E., Calder, A.G., Flint, H.J., and Lobley, G.E. (2011). Rates of productionand utilization of lactate by microbial communities fromthe human colon. FEMS Microbiol. Ecol. *77*, 107–119, 10.1111/j.1574-6941.2011.01086.x.

Brugiroux, S., Beutler, M., Pfann, C., Garzetti, D., Ruscheweyh, H.J., Ring, D., Diehl, M., Herp, S., Lotscher, Y., Hussain, S., et al. (2016). Genome-guided design of a defined mouse microbiota that confers colonization resistance against Salmonella enterica serovar Typhimurium. Nat Microbiol *2*, 16215, 10.1038/nmicrobiol.2016.215.

Butler, A.A., and Kozak, L.P. (2010). A recurring problem with the analysis of energy expenditure in genetic models expressing lean and obese phenotypes. Diabetes *59*, 323–329, 10.2337/db09-1471.

Caesar, R., Tremaroli, V., Kovatcheva-Datchary, P., Cani, P.D., and Bäckhed, F. (2015). Crosstalk between Gut Microbiota and Dietary Lipids Aggravates WAT Inflammation through TLR Signaling. Cell Metab. *22*, 658–668, 10.1016/J.CMET.2015.07.026.

Cai, T.Q., Ren, N., Jin, L., Cheng, K., Kash, S., Chen, R., Wright, S.D., Taggart, A.K.P., and Waters, M.G. (2008). Role of GPR81 in lactate-mediated reduction of adipose lipolysis. Biochem.

Biophys. Res. Commun. *377*, 987–991, 10.1016/j.bbrc.2008.10.088.

Cani, P.D., Van Hul, M., Lefort, C., Depommier, C., Rastelli, M., and Everard, A. (2019). Microbial regulation of organismal energy homeostasis. Nat. Metab. *1*, 34–46, 10.1038/s42255-018-0017-4.

Chong, J., and Xia, J. (2018). MetaboAnalystR: an R package for flexible and reproducible analysis of metabolomics data. Bioinformatics *34*, 4313–4314, 10.1093/bioinformatics/bty528.

Claus, S.P., Tsang, T.M., Wang, Y., Cloarec, O., Skordi, E., Martin, F.-P., Rezzi, S., Ross, A., Kochhar, S., Holmes, E., et al. (2008). Systemic multicompartmental effects of the gut microbiome on mouse metabolic phenotypes. Mol. Syst. Biol. *4*, 219, 10.1038/msb.2008.56.

Corrigan, J.K., Ramachandran, D., He, Y., Palmer, C.J., Jurczak, M.J., Chen, R., Li, B., Friedline, R.H., Kim, J.K., Ramsey, J.J., et al. (2020). A big-data approach to understanding metabolic rate and response to obesity in laboratory mice. Elife *9*, 10.7554/elife.53560.

Dennis, P.P., and Bremer, H. (2008). Modulation of Chemical Composition and Other Parameters of the Cell at Different Exponential Growth Rates. EcoSal Plus *3*, 10.1128/ecosal.5.2.3.

Doi, R., Oishi, K., and Ishida, N. (2010). CLOCK regulates circadian rhythms of hepatic glycogen synthesis through transcriptional activation of Gys2. J. Biol. Chem. *285*, 22114–22121, 10.1074/jbc.M110.110361.

Duncan, S.H., Louis, P., and Flint, H.J. (2004). Lactate-utilizing bacteria, isolated from human feces, that produce butyrate as a major fermentation product. Appl. Environ. Microbiol. *70*, 5810–5817, 10.1128/AEM.70.10.5810-5817.2004.

Eberl, C., Ring, D., Münch, P.C., Beutler, M., Basic, M., Slack, E.C., Schwarzer, M., Srutkova, D., Lange, A., Frick, J.S., et al. (2020). Reproducible Colonization of Germ-Free Mice With the Oligo-Mouse-Microbiota in Different Animal Facilities. Front. Microbiol. *10*, 2999, 10.3389/fmicb.2019.02999.

Faith, J.J., Ahern, P.P., Ridaura, V.K., Cheng, J., and Gordon, J.I. (2014). Identifying gut microbe-host phenotype relationships using combinatorial communities in gnotobiotic mice. Sci. Transl. Med. *6*, 220ra11-220ra11, 10.1126/scitranslmed.3008051.

Fernández-Verdejo, R., Ravussin, E., Speakman, J.R., and Galgani, J.E. (2019). Progress and challenges in analyzing rodent energy expenditure. Nat. Methods *16*, 797–799, 10.1038/s41592-019-0513-9.

Fetissov, S.O. (2017). Role of the gut microbiota in host appetite control: Bacterial growth to animal feeding behaviour. Nat. Rev. Endocrinol. *13*, 11–25, 10.1038/nrendo.2016.150.

Fleissner, C.K., Huebel, N., El-Bary, M.M.A., Loh, G., Klaus, S., and Blaut, M. (2010). Absence of intestinal microbiota does not protect mice from diet-induced obesity. Br. J. Nutr. *104*, 919–929,

10.1017/S0007114510001303.

Flint, H.J., Duncan, S.H., Scott, K.P., and Louis, P. (2015). Links between diet, gut microbiota composition and gut metabolism. Proc. Nutr. Soc. *74*, 13–22, 10.1017/S0029665114001463.

Gordon, H.A., and Pesti, L. (1971). The gnotobiotic animal as a tool in the study of host microbial relationships. Bact. Rev. *35*, 390–429, 10.1126/science.173.3992.171.

Goswami, C., Iwasaki, Y., and Yada, T. (2018). Short-chain fatty acids suppress food intake by activating vagal afferent neurons. J. Nutr. Biochem. *57*, 130–135, 10.1016/j.jnutbio.2018.03.009.

Halatchev, I.G., O'Donnell, D., Hibberd, M.C., and Gordon, J.I. (2019). Applying indirect open-circuit calorimetry to study energy expenditure in gnotobiotic mice harboring different human gut microbial communities. Microbiome *7*, 158, 10.1186/s40168-019-0769-4.

Harley, I.T.W., and Karp, C.L. (2012). Obesity and the gut microbiome: Striving for causality. Mol. Metab. *1*, 21–31, 10.1016/j.molmet.2012.07.002.

Ishikawa, K., and Shimazu, T. (1976). Daily rhythms of glycogen synthetase and phosphorylase activities in rat liver: influence of food and light. Life Sci. *19*, 1873–1878, 10.1016/0024-3205(76)90119-3.

Kaiyala, K.J., and Schwartz, M.W. (2011). Toward a more complete (and less controversial) understanding of energy expenditure and its role in obesity pathogenesis. Diabetes *60*, 17–23, 10.2337/db10-0909.

Koh, A., and Bäckhed, F. (2020). From Association to Causality: the Role of the Gut Microbiota and Its Functional Products on Host Metabolism. Mol. Cell *78*, 584–596, 10.1016/j.molcel.2020.03.005.

Kovatcheva-Datchary, P., Shoaie, S., Lee, S., Wahlström, A., Nookaew, I., Hallen, A., Perkins, R., Nielsen, J., and Bäckhed, F. (2019). Simplified Intestinal Microbiota to Study Microbe-Diet-Host Interactions in a Mouse Model. Cell Rep. *26*, 3772-3783.e6, 10.1016/j.celrep.2019.02.090.

Krisko, T.I., Nicholls, H.T., Bare, C.J., Holman, C.D., Putzel, G.G., Jansen, R.S., Sun, N., Rhee, K.Y., Banks, A.S., and Cohen, D.E. (2020). Dissociation of Adaptive Thermogenesis from Glucose Homeostasis in Microbiome-Deficient Mice. Cell Metab. *31*, 592-604.e9, 10.1016/J.CMET.2020.01.012.

Kuang, Z., Wang, Y., Li, Y., Ye, C., Ruhn, K.A., Behrendt, C.L., Olson, E.N., and Hooper, L. V. (2019). The intestinal microbiota programs diurnal rhythms in host metabolism through histone deacetylase 3. Science *365*, 1428–1434, 10.1126/science.aaw3134.

Kübeck, R., Bonet-Ripoll, C., Hoffmann, C., Walker, A., Müller, V.M., Schüppel, V.L., Lagkouvardos, I., Scholz, B., Engel, K.-H., Daniel, H., et al. (2016). Dietary fat and gut microbiota interactions determine diet-induced obesity in mice. Mol. Metab. *5*, 1162–1174,

10.1016/j.molmet.2016.10.001.

Levenson, S.M. (1978). The influence of the indigenous microflora on mammalian metabolism and nutrition. JPEN. J. Parenter. Enteral Nutr. *2*, 78–107, 10.1177/014860717800200203.

Levenson, S.M., Doft, F., Lev, M., and Kan, D. (1969). Influence of microorganisms on oxygen consumption, carbon dioxide production and colonic temperature of rats. J. Nutr. *97*, 542–552, 10.1093/jn/97.4.542.

Li, B., Li, L., Li, M., Lam, S.M., Wang, G., Wu, Y., Zhang, H., Niu, C., Zhang, X., Liu, X., et al. (2019). Microbiota Depletion Impairs Thermogenesis of Brown Adipose Tissue and Browning of White Adipose Tissue. Cell Rep. *26*, 2720-2737.e5, 10.1016/j.celrep.2019.02.015.

Li, M., Li, L., Li, B., Hambly, C., Wang, G., Wu, Y., Jin, Z., Wang, A., Niu, C., Wolfrum, C., et al. (2021). Brown adipose tissue is the key depot for glucose clearance in microbiota depleted mice. Nat. Commun. *12*, 1–13, 10.1038/s41467-021-24659-8.

Liebisch, G., Ecker, J., Roth, S., Schweizer, S., Öttl, V., Schött, H.F., Yoon, H., Haller, D., Holler, E., Burkhardt, R., et al. (2019). Quantification of fecal short chain fatty acids by liquid chromatography tandem mass spectrometry—investigation of pre-analytic stability. Biomolecules *9*, 121, 10.3390/biom9040121.

Lin, H. V., Frassetto, A., Kowalik Jr, E.J., Nawrocki, A.R., Lu, M.M., Kosinski, J.R., Hubert, J.A., Szeto, D., Yao, X., Forrest, G., et al. (2012). Butyrate and Propionate Protect against Diet-Induced Obesity and Regulate Gut Hormones via Free Fatty Acid Receptor 3-Independent Mechanisms. PLoS One *7*, e35240, 10.1371/journal.pone.0035240.

Liu, C., Wu, J., Zhu, J., Kuei, C., Yu, J., Shelton, J., Sutton, S.W., Li, X., Su, J.Y., Mirzadegan, T., et al. (2009). Lactate inhibits lipolysis in fat cells through activation of an orphan G-protein-coupled receptor, GPR81. J. Biol. Chem. *284*, 2811–2822, 10.1074/jbc.M806409200.

MacLean, P.S., Blundell, J.E., Mennella, J.A., and Batterham, R.L. (2017). Biological control of appetite: A daunting complexity. Obesity *25*, S8–S16, 10.1002/oby.21771.

Mallapaty, S. (2017). Gnotobiotics: getting a grip on the microbiome boom. Lab Anim. (NY). *46*, 373–377, 10.1038/laban.1344.

Mardinoglu, A., Shoaie, S., Bergentall, M., Ghaffari, P., Zhang, C., Larsson, E., Bäckhed, F., and Nielsen, J. (2015). The gut microbiota modulates host amino acid and glutathione metabolism in mice. Mol. Syst. Biol. *11*, 834, 10.15252/MSB.20156487.

Meyer, C.W., Reitmeir, P., and Tschop, M.H. (2015). Exploration of Energy Metabolism in the Mouse Using Indirect Calorimetry: Measurement of Daily Energy Expenditure (DEE) and Basal Metabolic Rate (BMR). Curr Protoc Mouse Biol *5*, 205–222, 10.1002/9780470942390.mo140216.

Mina, A.I., LeClair, R.A., LeClair, K.B., Cohen, D.E., Lantier, L., and Banks, A.S. (2018). CalR: A

Web-Based Analysis Tool for Indirect Calorimetry Experiments. Cell Metab. *28*, 656–666, 10.1016/j.cmet.2018.06.019.

Moor, K., Fadlallah, J., Toska, A., Sterlin, D., Balmer, M.L., Macpherson, A.J., Gorochov, G., Larsen, M., and Slack, E. (2016). Analysis of bacterial-surface-specific antibodies in body fluids using bacterial flow cytometry. Nat Protoc *11*, 1531–1553, 10.1038/nprot.2016.091.

Murtagh, F., and Legendre, P. (2014). Ward's Hierarchical Agglomerative Clustering Method: Which Algorithms Implement Ward's Criterion? J. Classif. 2014 313 *31*, 274–295, 10.1007/S00357-014-9161-Z.

Nowak, N. (2021). Metabolic Insights Related to Sleep and Circadian Clocks from Mass Spectrometry-Based Analysis of Blood and Breath. 10.3929/ETHZ-B-000480810.

Packard, G.C., and Boardman, T.J. (1999). The use of percentages and size-specific indices to normalize physiological data for variation in body size: Wasted time, wasted effort? Comp. Biochem. Physiol. - A Mol. Integr. Physiol. *122*, 37–44, 10.1016/S1095-6433(98)10170-8.

Popovic, M. (2019). Thermodynamic properties of microorganisms: determination and analysis of enthalpy, entropy, and Gibbs free energy of biomass, cells and colonies of 32 microorganism species. Heliyon *5*, e01950, 10.1016/j.heliyon.2019.e01950.

Rabasa, C., and Dickson, S.L. (2016). Impact of stress on metabolism and energy balance. Curr. Opin. Behav. Sci. *9*, 71–77, 10.1016/J.COBEHA.2016.01.011.

Ridaura, V.K., Faith, J.J., Rey, F.E., Cheng, J., Duncan, A.E., Kau, A.L., Griffin, N.W., Lombard, V., Henrissat, B., Bain, J.R., et al. (2013). Gut microbiota from twins discordant for obesity modulate metabolism in mice. Science *341*, 1241214, 10.1126/science.1241214.

Sayin, S.I., Wahlström, A., Felin, J., Jäntti, S., Marschall, H.U., Bamberg, K., Angelin, B., Hyötyläinen, T., Orešič, M., and Bäckhed, F. (2013). Gut microbiota regulates bile acid metabolism by reducing the levels of tauro-beta-muricholic acid, a naturally occurring FXR antagonist. Cell Metab. *17*, 225–235, 10.1016/j.cmet.2013.01.003.

Schmidt, T.S.B., Raes, J., and Bork, P. (2018). The Human Gut Microbiome: From Association to Modulation. Cell *172*, 1198–1215, 10.1016/j.cell.2018.02.044.

von Schwartzenberg, R.J., Bisanz, J.E., Lyalina, S., Spanogiannopoulos, P., Ang, Q.Y., Cai, J., Dickmann, S., Friedrich, M., Liu, S.-Y., Collins, S.L., et al. (2021). Caloric restriction disrupts the microbiota and colonization resistance. Nature 1–6, 10.1038/s41586-021-03663-4.

Smith, C.A., Want, E.J., O'Maille, G., Abagyan, R., and Siuzdak, G. (2006). XCMS: processing mass spectrometry data for metabolite profiling using nonlinear peak alignment, matching, and identification. Anal. Chem. *78*, 779–787, 10.1021/ac051437y.

Sonnenburg, J.L., and Bäckhed, F. (2016). Diet-microbiota interactions as moderators of human

metabolism. Nature *535*, 56–64, 10.1038/nature18846.

Speakman, J.R. (2013). Measuring energy metabolism in the mouse - theoretical, practical, and analytical considerations. Front Physiol *4*, 34, 10.3389/fphys.2013.00034.

Steimle, A., De Sciscio, A., Neumann, M., Grant, E.T., Pereira, G. V., Ohno, H., Martens, E.C., and Desai, M.S. (2021). Constructing a gnotobiotic mouse model with a synthetic human gut microbiome to study host–microbe cross talk. STAR Protoc. *2*, 100607, 10.1016/J.XPRO.2021.100607.

Streidl, T., Karkossa, I., Segura Muñoz, R.R., Eberl, C., Zaufel, A., Plagge, J., Schmaltz, R., Schubert, K., Basic, M., Schneider, K.M., et al. (2021). The gut bacterium Extibacter muris produces secondary bile acids and influences liver physiology in gnotobiotic mice. Gut Microbes *13*, 1–21, 10.1080/19490976.2020.1854008.

Stubbs, R.J., Hopkins, M., Finlayson, G.S., Duarte, C., Gibbons, C., and Blundell, J.E. (2018). Potential effects of fat mass and fat-free mass on energy intake in different states of energy balance. Eur. J. Clin. Nutr. *72*, 698–709, 10.1038/s41430-018-0146-6.

Suárez-Zamorano, N., Fabbiano, S., Chevalier, C., Stojanović, O., Colin, D.J., Stevanović, A., Veyrat-Durebex, C., Tarallo, V., Rigo, D., Germain, S., et al. (2015). Microbiota depletion promotes browning of white adipose tissue and reduces obesity. Nat. Med. *21*, 1497–1501, 10.1038/nm.3994.

Tahara, Y., Yamazaki, M., Sukigara, H., Motohashi, H., Sasaki, H., Miyakawa, H., Haraguchi, A., Ikeda, Y., Fukuda, S., and Shibata, S. (2018). Gut Microbiota-Derived Short Chain Fatty Acids Induce Circadian Clock Entrainment in Mouse Peripheral Tissue. Sci. Rep. *8*, 1395, 10.1038/s41598-018-19836-7.

Tanner, J.M. (1949). Fallacy of per-weight and per-surface area standards, and their relation to spurious correlation. J. Appl. Physiol. *2*, 1–15, 10.1152/jappl.1949.2.1.1.

Thaiss, C.A., Zeevi, D., Levy, M., Zilberman-Schapira, G., Suez, J., Tengeler, A.C., Abramson, L., Katz, M.N., Korem, T., Zmora, N., et al. (2014). Transkingdom control of microbiota diurnal oscillations promotes metabolic homeostasis. Cell *159*, 514–529, 10.1016/j.cell.2014.09.048.

Thaiss, C.A., Levy, M., Korem, T., Dohnalova, L., Shapiro, H., Jaitin, D.A., David, E., Winter, D.R., Gury-BenAri, M., Tatirovsky, E., et al. (2016). Microbiota Diurnal Rhythmicity Programs Host Transcriptome Oscillations. Cell *167*, 1495-1510 e12, 10.1016/j.cell.2016.11.003.

Touw, K., Ringus, D.L., Hubert, N., Wang, Y., Leone, V.A., Nadimpalli, A., Theriault, B.R., Huang, Y.E., Tune, J.D., Herring, P.B., et al. (2017). Mutual reinforcement of pathophysiological host-microbe interactions in intestinal stasis models. Physiol. Rep. *5*, e13182, 10.14814/PHY2.13182.

Tschop, M.H., Speakman, J.R., Arch, J.R., Auwerx, J., Bruning, J.C., Chan, L., Eckel, R.H., Farese Jr., R. V, Galgani, J.E., Hambly, C., et al. (2011). A guide to analysis of mouse energy metabolism.

Nat Methods *9*, 57–63, 10.1038/nmeth.1806.

Turnbaugh, P.J., Ley, R.E., Mahowald, M.A., Magrini, V., Mardis, E.R., and Gordon, J.I. (2006). An obesity-associated gut microbiome with increased capacity for energy harvest. Nature *444*, 1027–1031, 10.1038/nature05414.

Ucar, I., Pebesma, E., and Azcorra, A. (2019). Measurement errors in R. R J. *10*, 549–557, 10.32614/RJ-2018-075.

Walter, J., Armet, A.M., Finlay, B.B., and Shanahan, F. (2020). Establishing or Exaggerating Causality for the Gut Microbiome: Lessons from Human Microbiota-Associated Rodents. Cell *180*, 221–232, 10.1016/j.cell.2019.12.025.

Wang, Y., Kuang, Z., Yu, X., Ruhn, K.A., Kubo, M., and Hooper, L. V. (2017). The intestinal microbiota regulates body composition through NFIL3 and the circadian clock. Science *357*, 912–916, 10.1126/science.aan0677.

Weir, J.B.D.B. (1949). New methods for calculating metabolic rate with special reference to protein metabolism. J. Physiol. *109*, 1–9, 10.1113/jphysiol.1949.sp004363.

Weiss, A.S., Burrichter, A.G., Chakravarthy, A., Raj, D., Von Strempel, A., Meng, C., Kleigrewe, K., Münch, P.C., Rössler, L., Huber, C., et al. (2021). In vitro interaction network of a synthetic gut bacterial community. ISME J. 2021 1–15, 10.1038/s41396-021-01153-z.

White, C.R., and Seymour, R.S. (2005). Allometric scaling of mammalian metabolism. J. Exp. Biol. *208*, 1611–1619, 10.1242/jeb.01501.

Wostmann, B.S., Bruckner-Kardoss, E., and Knight, P.L. (1968). Cecal Enlargement, Cardiac Output, and O2 Consumption in Germfree Rats. Exp. Biol. Med. *128*, 137–141, 10.3181/00379727-128-32962.

Wostmann, B.S., Larkin, C., Moriarty, A., and Bruckner-Kardoss, E. (1983). Dietary intake, energy metabolism, and excretory losses of adult male germfree Wistar rats. Lab. Anim. Sci. *33*, 46–50.

Woting, A., Pfeiffer, N., Loh, G., Klaus, S., and Blaut, M. (2014). Clostridium ramosum promotes High-Fat diet-induced obesity in Gnotobiotic Mouse Models. MBio *5*, 1530–1544, 10.1128/mBio.01530-14.

Woting, A., Pfeiffer, N., Hanske, L., Loh, G., Klaus, S., and Blaut, M. (2015). Alleviation of high fat diet-induced obesity by oligofructose in gnotobiotic mice is independent of presence of Bifidobacterium longum. Mol. Nutr. Food Res. *59*, 2267–2278, 10.1002/mnfr.201500249.

Wotzka, S.Y., Kreuzer, M., Maier, L., Arnoldini, M., Nguyen, B.D., Brachmann, A.O., Berthold, D.L., Zünd, M., Hausmann, A., Bakkeren, E., et al. (2019). Escherichia coli limits Salmonella Typhimurium infections after diet shifts and fat-mediated microbiota perturbation in mice. Nat. Microbiol. 10.1038/s41564-019-0568-5.

Yao, L., Seaton, S.C., Ndousse-Fetter, S., Adhikari, A.A., DiBenedetto, N., Mina, A.I., Banks, A.S., Bry, L., and Devlin, A.S. (2018). A selective gut bacterial bile salt hydrolase alters host metabolism. Elife *7*, 10.7554/eLife.37182.

Yilmaz, B., Mooser, C., Keller, I., Li, H., Zimmermann, J., Bosshard, L., Fuhrer, T., Gomez de Agüero, M., Trigo, N.F., Tschanz-Lischer, H., et al. (2021). Long-term evolution and short-term adaptation of microbiota strains and sub-strains in mice. Cell Host Microbe *29*, 650-663.e9, 10.1016/j.chom.2021.02.001.

Zarrinpar, A., Chaix, A., Yooseph, S., and Panda, S. (2014). Diet and feeding pattern affect the diurnal dynamics of the gut microbiome. Cell Metab. *20*, 1006–1017, 10.1016/j.cmet.2014.11.008.

Zarrinpar, A., Chaix, A., Xu, Z.Z., Chang, M.W., Marotz, C.A., Saghatelian, A., Knight, R., and Panda, S. (2018). Antibiotic-induced microbiome depletion alters metabolic homeostasis by affecting gut signaling and colonic metabolism. Nat. Commun. 2018 91 *9*, 1–13, 10.1038/s41467-018-05336-9.

SUPPLEMENTARY TABLE

Supplementary Table 1. List of metabolites identified by targeted peak extraction in the UPLC/MS data. Table indicates compound name, KEGG Entry number, type of column was used for UPLC and if the peak ID matched the retention time and MS2 spectra identified with the chemical standard in liver and plasma samples.

Compound	**KEGG Entry**	**Column**	**Matched peak ID in Liver**	**Matched peak ID in Plasma**
(R)-3-hydroxybutanic acid	C01089	RP Negative	Yes	No
5-Oxoproline	C01879	AMIDE Positive	Yes	Yes
Arachidonic acid	C00219	RP Negative	Yes	Yes
Betaine	C00719	AMIDE Positive	No	Yes
beta-Murocholic acid	C17726	RP Negative	Yes	Yes
Cholic acid	C00695	RP Negative	Yes	Yes
Citrulline	C00327	AMIDE Positive	Yes	Yes
Cortisol	C00735	RP Positive	Yes	No
Creatine	C00300	AMIDE Positive	Yes	Yes

Creatinine	C00791	AMIDE Positive	No	Yes
Cystathionine	C02291	AMIDE Positive	Yes	Yes
Deoxycholic acid	C04483	RP Negative	No	Yes
Docosapentaenoic acid	C16513	RP Negative	Yes	Yes
Glutathione (GSH)	C00051	AMIDE Positive	No	Yes
Glycine	C00037	AMIDE Positive	Yes	Yes
Glycocholic acid	C01921	RP Positive	Yes	No
Hexadecanedioic acid		RP Negative	Yes	Yes
Hippuric acid	C01586	RP Negative	Yes	Yes
L-(+)-Ornithine	C00077	AMIDE Positive	Yes	Yes
L-4-Hydroxyproline	C01157	AMIDE Positive	Yes	Yes
L-Alanine	C00041	AMIDE Positive	Yes	Yes
L-Arginine	C00062	AMIDE Positive	Yes	Yes
Lauroylcarnitine		RP Positive	Yes	Yes

Leucine	C00123	RP Positive	Yes	Yes
L-Glutamic acid	C00025	AMIDE Positive	Yes	Yes
L-Histidine	C00135	AMIDE Positive	Yes	Yes
Linoleic acid	C01595	RP Negative	Yes	Yes
L-Isoleucine	C00407	RP Positive	Yes	Yes
L-Lysine	C00047	AMIDE Positive	Yes	Yes
L-Methionine	C00073	AMIDE Positive	Yes	Yes
L-Proline	C00148	AMIDE Positive	Yes	Yes
L-Serine	C00065	AMIDE Positive	Yes	Yes
L-Threonine	C00188	AMIDE Positive	Yes	Yes
L-Tryptophan	C00078	RP Negative	Yes	Yes
L-Tyrosine	C00082	RP Negative	Yes	Yes
Myristic acid	C06424	RP Negative	Yes	Yes
N,N-dimethylglycine	C01026	AMIDE Positive	Yes	Yes

N-Acetylmethionine	C02712	RP Positive/Negative	Yes	Yes
Oxidized glutathione (GSSG)	C00127	AMIDE Negative	Yes	Yes
Pantothenic acid	C00864	RP Positive	Yes	Yes
Pipecolinic acid	C00408	RP Positive	Yes	Yes
Serotonin	C00780	RP Positive	Yes	Yes
Succinic acid	C00042	RP Negative	Yes	Yes
Taurine	C00245	AMIDE Negative	Yes	Yes
Taurine-beta-murocholic acid		AMIDE Negative	Yes	Yes
Taurochenodeoxycholic acid	C05465	AMIDE Negative	Yes	Yes
Tetradecanedioic acid		RP Negative	Yes	Yes

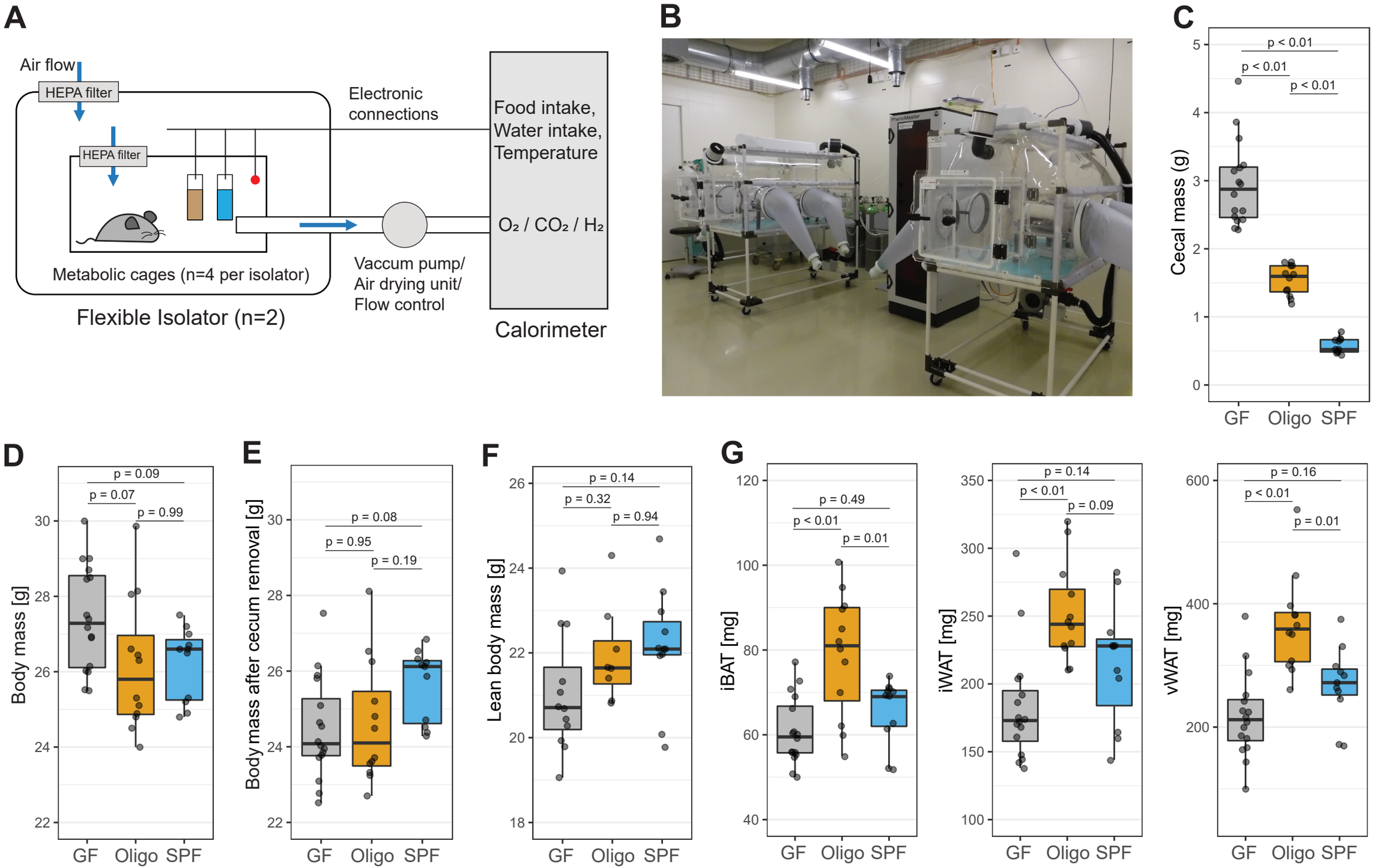

Figure 1: OligoMM12 mice have increase fat mass compared to GF mice and SPF C57B6/J mice.

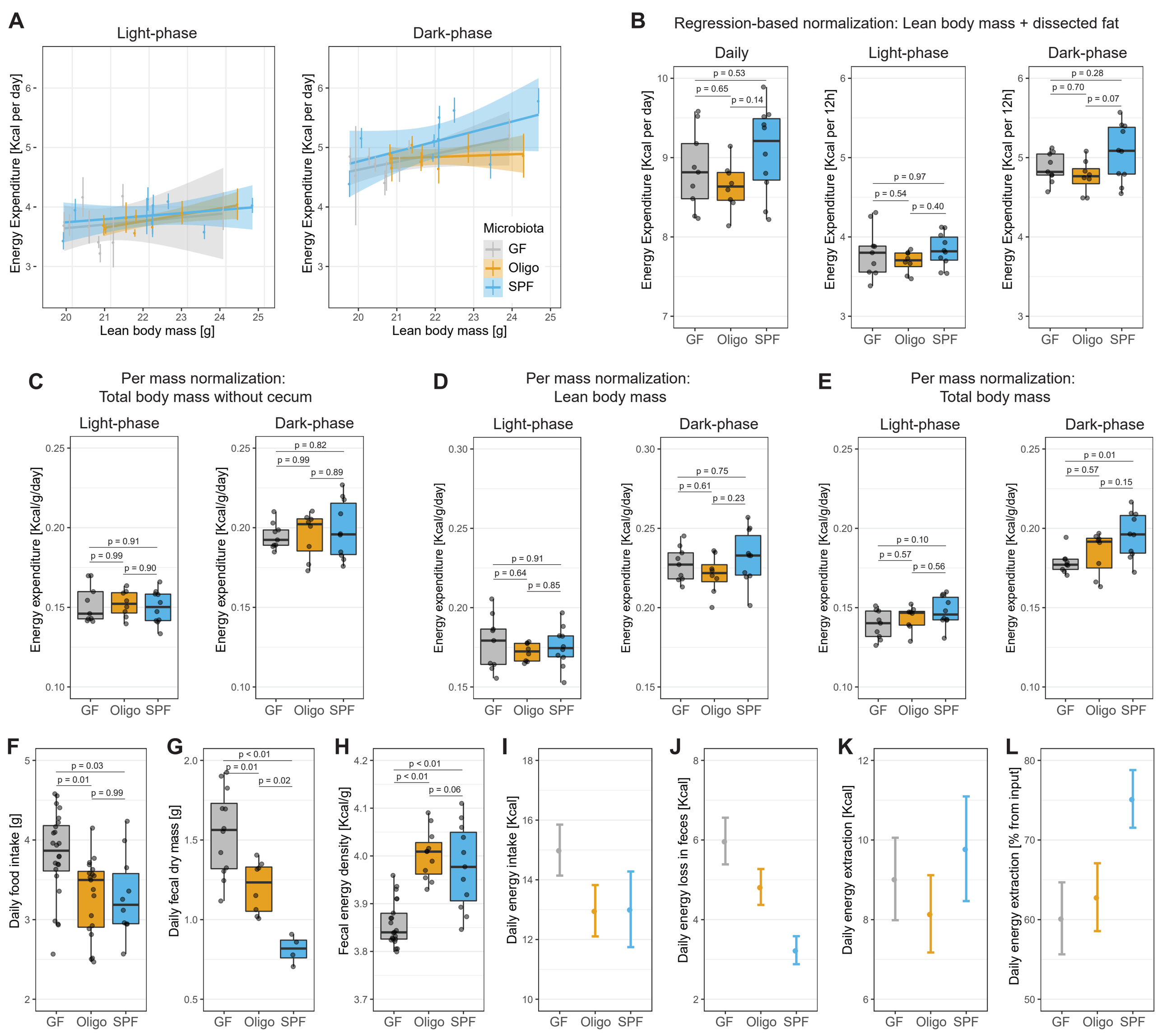

Figure 2: Energy metabolism in GF, OligoMM12 and SPF C57B6/J mice.

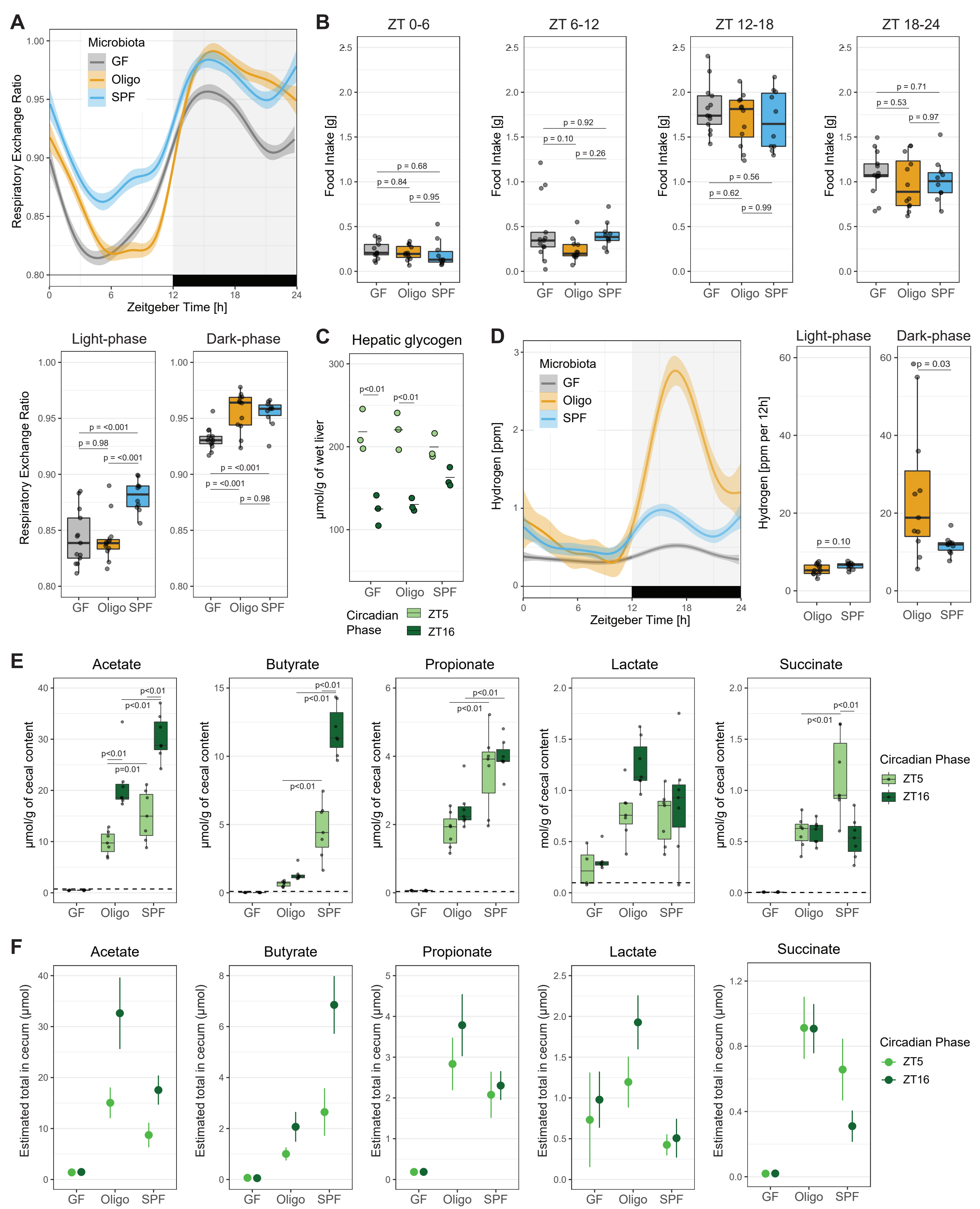

Figure 3: Circadian changes in Respiratory Exchange Ratio (RER), microbiota-derived hydrogen and short-chain fatty acids (SCFAs).

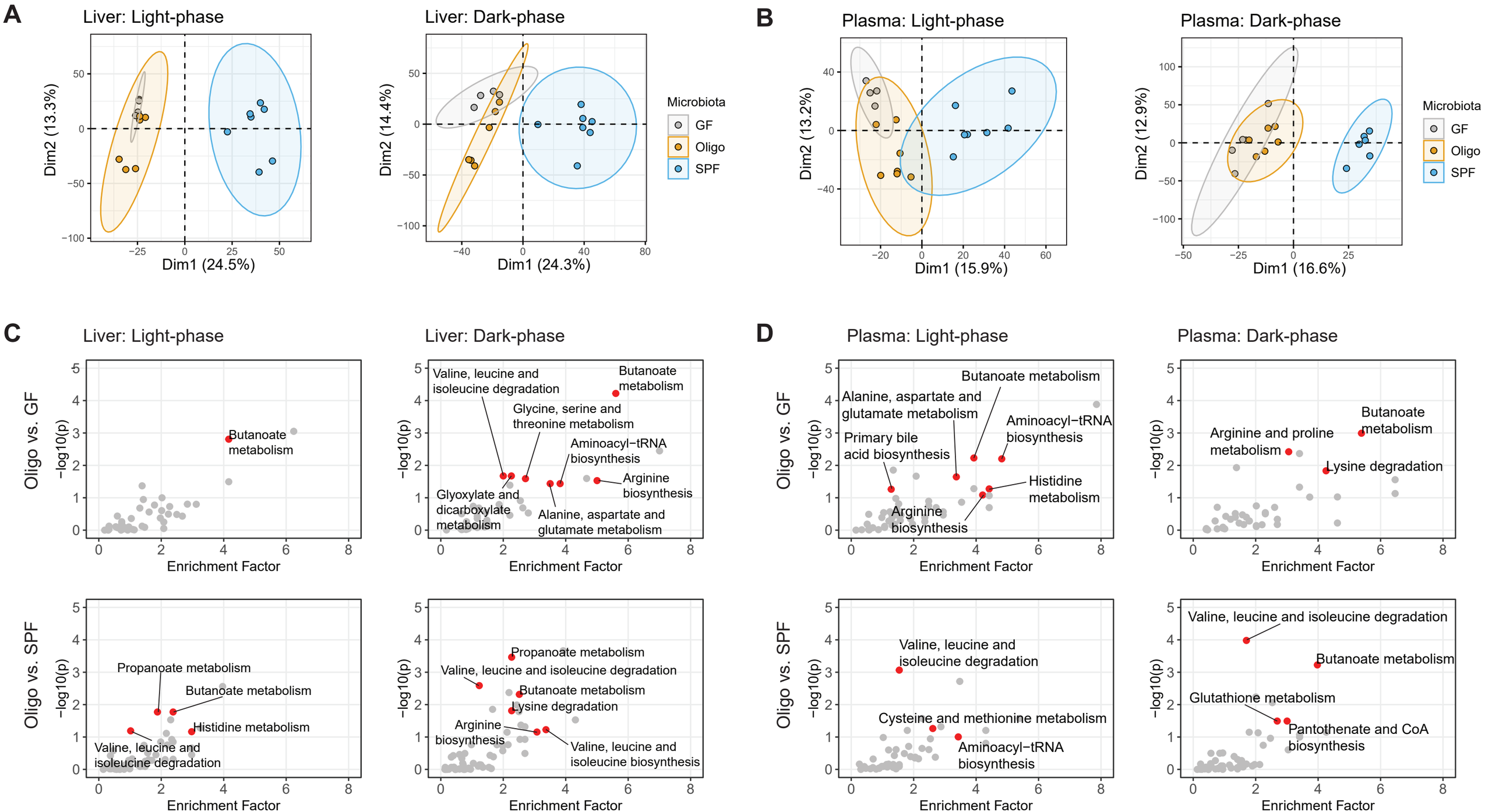

Figure 4. Metabolic profile comparison of GF, OligoMM12 and SPF mice by UPLC/MS.

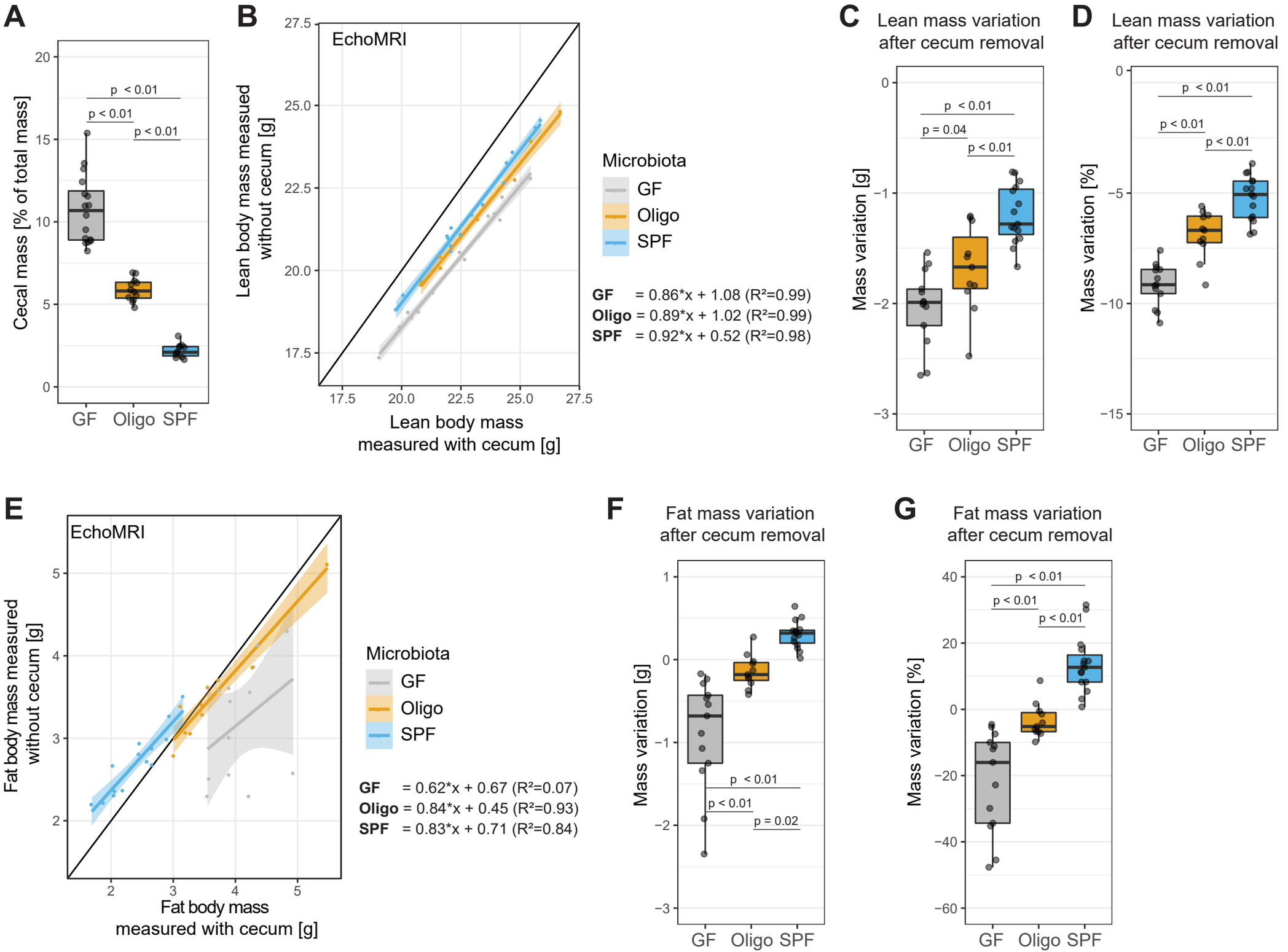

Supplementary Figure 1: Cecal mass interferes with fat mass estimation by Echo-MRI.

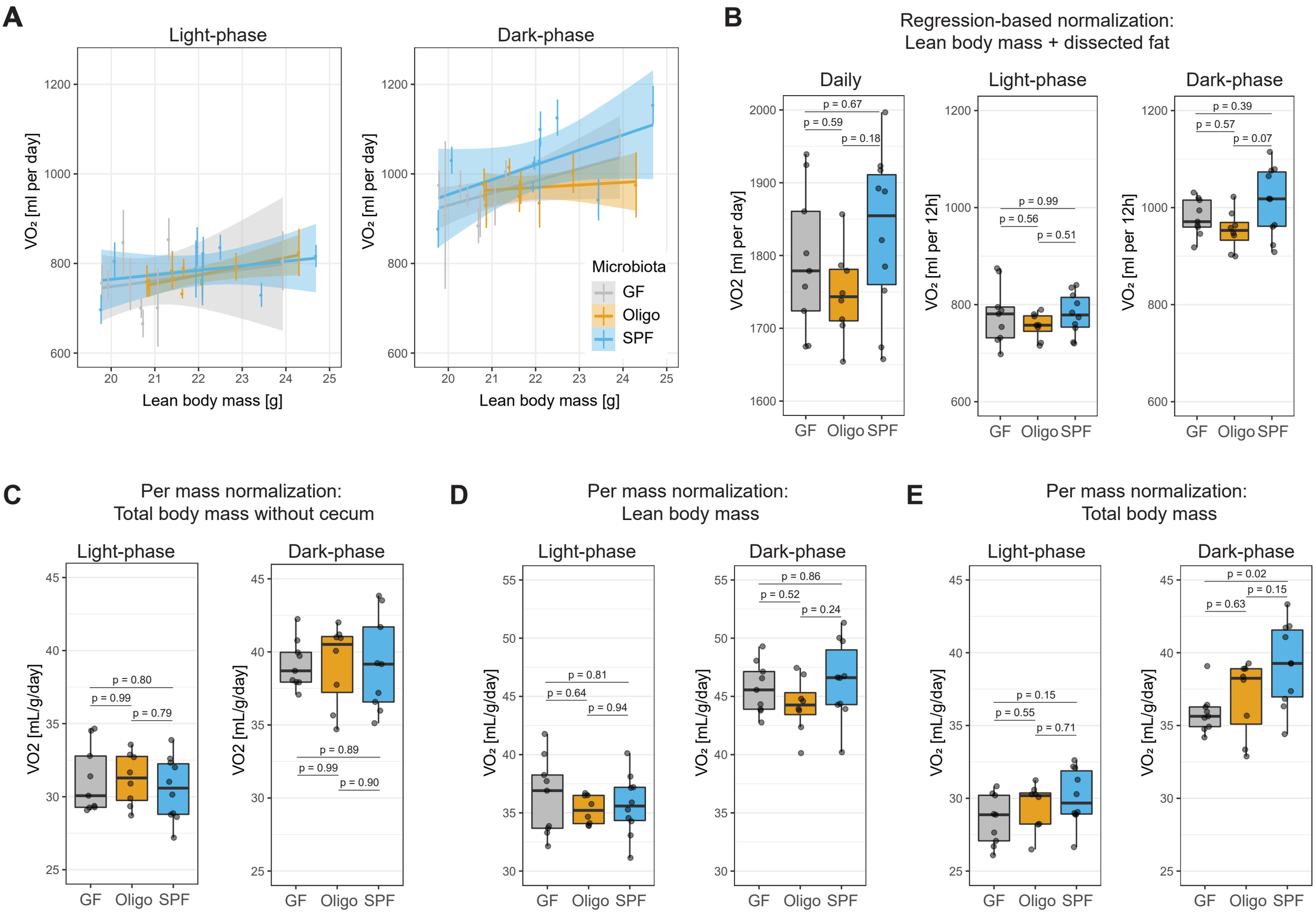

Supplementary Figure 2: Cecal mass interferes with normalization of VO2 and Energy Expenditure.

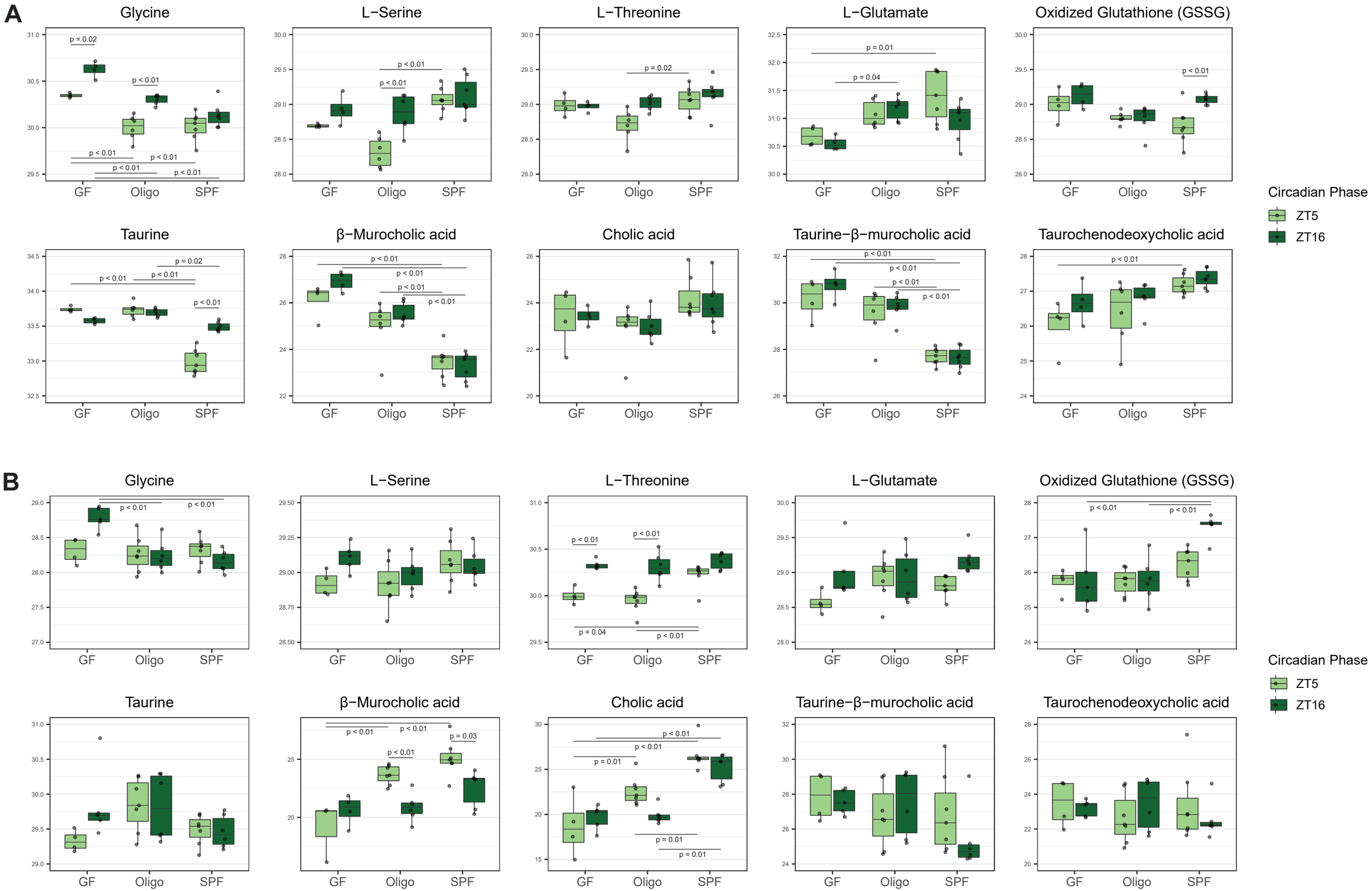

Supplementary Figure 3. Metabolic profile comparison of GF, OligoMM12 and SPF mice by UPLC/MS (targeted peak extraction of selected list of compounds)